Universidade do Minho
Escola de Engenharia

Vítor Hugo Moura Guedes

Airflow simulation in a horizontal closed refrigerated display cabinet

Master's Dissertation in Mechanical Engineer

Work developed under supervision of

Professor Doutor Pedro Alexandre Moreira Lobarinhas

Professora Doutora Senhorinha de Fátima Capela Fortunas Teixeira

July 2019

DIREITOS DE AUTOR E CONDIÇÕES DE UTILIZAÇÃO DO TRABALHO POR TERCEIROS

Este é um trabalho académico que pode ser utilizado por terceiros desde que respeitadas as regras e boas práticas internacionalmente aceites, no que concerne aos direitos de autor e direitos conexos.

Assim, o presente trabalho pode ser utilizado nos termos previstos na licença abaixo indicada.

Caso o utilizador necessite de permissão para poder fazer um uso do trabalho em condições não previstas no licenciamento indicado, deverá contactar o autor, através do RepositóriUM da Universidade do Minho.

Licença concedida aos utilizadores deste trabalho

Atribuição

CC BY

https://creativecommons.org/licenses/by/4.0/

ACKNOWLEDGMENTS

To my tutors, Professor Pedro Lobarinhas, for all the knowledge and support provided, to Professor Senhorinha Teixeira, for the help and make me think a step ahead.

To Master João Vasconcelos, for following this project since its beginning and all the help especially with the software ANSYS – FLUENT.

To my family: my mother, my father and my brother, for making this project possible and all the support during it.

To my friends and colleagues that help me in many ways.

DECLARAÇÃO DE INTEGRIDADE

Declaro ter atuado com integridade na elaboração do presente trabalho académico e confirmo que não recorri à prática de plágio nem a qualquer forma de utilização indevida ou falsificação de informações ou resultados em nenhuma das etapas conducente à sua elaboração.

Mais declaro que conheço e que respeitei o Código de Conduta Ética da Universidade do Minho.

RESUMO

Os equipamentos de refrigeração tornaram-se essenciais em várias vertentes, especialmente na conservação de alimentos. Nos últimos anos os equipamentos de refrigeração fechados têm ganho destaque devido ao seu consumo ser muito inferior comparativamente com os abertos.

O estudo centra-se na análise do escoamento de ar frio que percorre o equipamento, tendo em conta as condições exteriores. Para este efeito recorreu-se ao uso do programa CFD ANSYS Fluent. Este usa a técnica de volumes finitos na solução das equações de conservação da massa, *momentum* e energia.

Na primeira parte do trabalho fez-se um conjunto de simulações 2D em que foram estudados vários parâmetros. Primeiramente, foi analisada a dimensão da malha mais adequada (com apenas elementos quadriláteros); de seguida, foi feita uma comparação entre diferentes tipos de saídas e modelos de turbulência. Para terminar o estudo 2D foram colocados produtos de diferentes dimensões, atuando como obstáculos ao escoamento.

Quanto à influência dos parâmetros, pode concluir-se que o mais predominante é a temperatura na zona inferior junto ao evaporador. O fluxo de calor junto à parede e a influência das lâmpadas na geometria com produtos afetam pontualmente, não se refletindo noutras zonas geometria de uma forma evidente. O aumento da área perfurada nas costas na zona inferior permite uma maior ventilação nessa zona, contudo a temperatura aumenta ligeiramente.

Quanto à geometria com produtos, pode concluir-se através dos resultados que a geometria 2D utilizada é bastante limitadora.

Palavras-Chave: Vitrine fechada, simulação CFD, escoamento de ar, ANSYS Fluent.

ABSTRACT

Refrigeration equipment has become essential in several areas, especially in food preservation. In the last few years, closed refrigeration equipment becomes more popular because its consumption is much lower compared to the open ones.

The work of this study focuses on the analysis of the cold air flow that traverses the equipment, knowing the external conditions. For this purpose, CFD ANSYS Fluent program was used. This uses the finite volumes technique to solve the equations of conservation of mass, *momentum* and energy.

In the first part of the work, it was made a set of 2D simulations in which several parameters were studied. Firstly, the most appropriate mesh dimension was analysed (using only quadrilateral elements), then a comparison was made between different types of exits and turbulence models. To finish the 2D study products were introduced in the geometry with different dimensions, acting as obstacles to the fluid flow.

Concerning the influence of the parameters, it can be concluded that the most predominant is the temperature in the lower zone near the evaporator. The heat flux near the wall and the influence of the lamps on the geometry with products affect punctually, not being reflected in other geometry zones significantly. The increased perforated area in the lower back allows greater ventilation in the lower back, however the temperature increases slightly.

In the geometry with products, it can be concluded that the 2D geometry used is very limiting.

Keywords: Closed display cabinet, CFD simulation, airflow, ANSYS Fluent

CONTENTS

Acknowledgments ..... **iii**

Declaração de integridade ..... **iv**

Resumo ..... **v**

Abstract ..... **vi**

Contents ..... **vii**

List of figures ..... **ix**

List of tables ..... **xii**

Nomenclature ..... **xiii**

List of symbols ..... **xiv**

1. Introduction **1**

1.1. Closed showcases 2

1.2. Objectives 3

1.3. Dissertation structure 4

2. State of art **6**

2.1. Problem description 7

2.2. Cold equipment classification 8

2.3. Literature review 9

3. Computational model **15**

3.1. Mathematical model 17

3.2. Turbulence models 24

3.3. Finite volumes 27

3.4. SIMPLE 29

3.5. Residual values and convergence 33

4. Case study 36

4.1. Strategies adopted 36

4.2. Mesh definition 38

4.3. Mesh optimization 40

5. Results and discussion 46

5.1. Study of some parameters influence 46

5.1.1. Boundary condition on the bottom boundary: 0°C 46

5.1.2. Heat flux 50 and 150W/m^{2}K 49

5.1.3. Back entrances double size bottom 50

5.2. Geometry with products inclusion and lamps influence 52

6. Conclusion and future work 56

6.1 Conclusions 56

6.2 Future work 57

7. References 58

LIST OF FIGURES

Figure 1.1 - example of food preservation equipment 1

Figure 1.2 - cold showcase description 3

Figure 2.1 - showcase's full scheme, including the cold production zone and the storage zone 6

Figure 2.2 – Real steam compression system 7

Figure 2.3 - Temperature field using multiple air curtains..... 10

Figure 2.4 - mean temperature and standard deviations of the display cabinet with doors (a) and without doors (b)..... 11

Figure 2.5 - Iced drink cabinet description,..... 12

Figure 2.6 - results at the end of each stage: (a) flow field, (b) temperature field..... 13

Figure 2.7 - Pathlines for plate evaporator, 1 - with a finned surface, 2 – without a finned surface 14

Figure 3.1 - Continuity on control volume, ... 18

Figure 3.2 - Conservation of momentum, ... 19

Figure 3.3 - Conservation of momentum in x 20

Figure 3.4 - Energy conservation,..... 23

Figure 3.5 – SST k-ω model definition..... 26

Figure 3.6 -Fluxes in a 2D element according to finite volumes method 28

Figure 3.7 - Nodes and vector designation in a 2D element according to finite volumes method 29

Figure 3.8 - Control volume..... 31

Figure 3.9 - Residual values definition on ANSYS - FLUENT 35

Figure 4.1 - Showcase's geometry with no products in the shelves 36

Figure 4.2 - Mesh definition near the glass and wall, element size = 1.65mm (mesh 4, approximately 230,000 elements) 39

Figure 4.3 - Temperature field after 60s in the meshes 1 to 5, T_0 = 15°C, v_0 = 2 m/s, T(inlet) = 0°C, Q(glass) = 8.29 W/m^{2}K 42

Figure 4.4 - Velocity field after 60s in the meshes 1 to 5, T_0 = 15°C, v_0 = 2m/s, T(inlet) = 0°C, Q(glass) = 8.29W/m^{2}K 43

Figure 4.6 - temperature field for mesh 3 after 60 seconds, T_0 = 15°C, v_0 = 2 m/s, T(inlet) = 0°C, Q(glass) = 8.29 W/m^{2}K 45

Figure 4.5 - temperature field for mesh 3 after 55 seconds, T_0 = 15°C, v_0 = 2m/s, T(inlet) = 0°C, Q(glass) = 8.29 W/m^{2}K 45

Figure 5.1 - definition of glass, inlet and outlet 47

Figure 5.2 – temperature field after 120s for meshes 4 and 5, T_0 = 15°C, v_0 = 2m/s, T(inlet) = 0°C, Q(glass) = 8.29 W/m^{2}K, T(bottom) = 0°C 47

Figure 5.3 - velocity field after 120s for meshes 4 and 5, T_0 = 15°C, v_0 = 2 m/s, T(inlet) = 0°C, Q(glass) = 8.29 W/m^{2}K, T(bottom) = 0°C 48

Figure 5.4 – glass boundary condition 49

Figure 5.5 - temperature field after 120s, T_0=15°C, v_0 = 2 m/s, T(inlet) = 0°C, Q(glass) = 8.29 W/m^{2}K, T(bottom) = 0°C 50

Figure 5.6 - temperature field after 120s, T_0 = 15°C, v_0 = 2 m/s, T(inlet)=0°C, Q(glass)=8.29 W/m^{2}K, T(bottom) = 0°C 50

Figure 5.7 - velocity field after 120s, T_0 = 15°C, v_0 = 2 m/s, T(inlet) = 0°C, Q(glass) = 8.29 W/m^{2}K, T(bottom) = 0°C, with double sized entrances on the bottom of the perforated plate 51

Figure 5.8 - temperature field after 120s, T_0 = 15°C, v_0 = 2 m/s, T(inlet) = 0°C, Q(glass) = 8.29 W/m^{2}K, T(bottom) = 0°C, with double sized entrances on the bottom of the perforated plate 51

Figure 5.9 - geometry with products 52

Figure 5.10 - mesh definition near the glass 53

Figure 5.11 - geometry with products, temperature field after 120s, T_0 = 15°C, v_0 = 2 m/s, T(inlet) = 0°C, Q(glass) = 8.29 W/m^{2}K, T(bottom) = 0°C, with double sized entrances on the bottom of the perforated plate 54

Figure 5.13 - geometry with products, velocity field after 120s, T_0 = 15°C, v_0 = 2m/s, T(inlet) = 0°C, Q(glass) = 8.29 W/m^{2}K, T(bottom) = 0°C, with double sized entrances on the bottom of the perforated plate 54

LIST OF TABLES

Table 2.1 - Classification of refrigerating equipment according to PRODCOM 8

Table 3.1 - Turbulence models description 25

Table 3.2 - Coefficients definition 32

Table 4.1 - Mesh quality report 40

NOMENCLATURE

CFD	*Computational Fluid Dynamics*
2D	*Two-dimensional*
3D	*Three-dimensional*
GWP	*Global Warming Potential*
ODP	*Ozone Depletion Rate*
PRODCOM	*PRODuction COMmunataire (community production)*

LIST OF SYMBOLS

ρ	Density	[kg/m^3]
τ	Surface stress	[Pa]
S	Source term	[-]
q	Heat flux	[W/m^2]
K	Turbulent kinetic energy	[-]
T	Temperature	[K]
Re	Reynolds number	[-]
A	Area	[m^2]
$\dot{m}$	Mass flow	[kg/s]
k	Thermal conductivity coefficient	[W/mK]
$\emptyset$	Volumetric flow rate	[m^3/s]

1. INTRODUCTION

Mankind has always used food preservation since its inception. A very effective way of preserving food is to keep them at low temperatures, avoiding the formation of microorganisms, thus preventing their degradation. Over the years, several refrigeration systems have been created and refined for this purpose, the first of which consisted of simple cabinets with ice cubes. Even today the refrigeration is the most common process to preserve the food, although refrigeration has many other applications, such as health care, space cooling (to increase processes efficiency or comfort), industry, etc. (figure 1.1). There are many ways to «produce cold» and many fluids that can be used for this purpose. In the past many fluids were used because of their high efficiency (CFC, HCFC). However, some of them were banned because of the environmental impact. There are two main coefficients to evaluate this impact: ODP (Ozone Depletion Potential) and GWP (Global Warming Potential). Today the legislation only allows fluids with ODP equal to zero and low GWP (this value oscillate depending on the equipment, the application and if it is commercial or domestic).

Figure 1.1 - example of food preservation equipment, from http://ingecold.com.br/novidades_detalhe.php?noticia=24

As already mentioned, the main concern nowadays with the use of cold equipment has to do with its energy expenditure. This implies the correct use of equipment (such as reducing the opening time of doors in a refrigerator/freezer), but

also a greater effort on the part of the manufacturers, who must guarantee the correct functioning of the equipment with the minimum power dissipated. For that reason, closed display cabinets become more and more popular over the years[1].

The most popular way to produce cold in these devices is using refrigerants, that will transport the heat from the cold source to the hot source. Depending on which source is the one is interested (to refrigerate is the cold source and to heating is the hot source), there are two different classifications: heat pumps (heating) and refrigeration machines (cooling). That the operation is the same for both, and there are many types of equipment that can do both tasks, such as air conditioners.

1.1. Closed showcases

Commercial refrigeration equipment is indispensable for the preservation of food in such establishments, namely butchers, bakeries, etc. A schematic drawing of the cabinet is presented in figure 1.2. There is an upwards airflow on the back that will be split in two: a fraction of this flow is entering on the equipment by the back perforated plated and the rest of it is entering on the top, near the glass on the front, forming an air curtain.

This type of equipment is divided into two zones: cold production and storage (figure 1.2). The cold production zone is usually located at the bottom of the equipment. This zone contains insulating material to prevent energy loss to the outside and there is only one connection to the storage zone to enable the airflow.

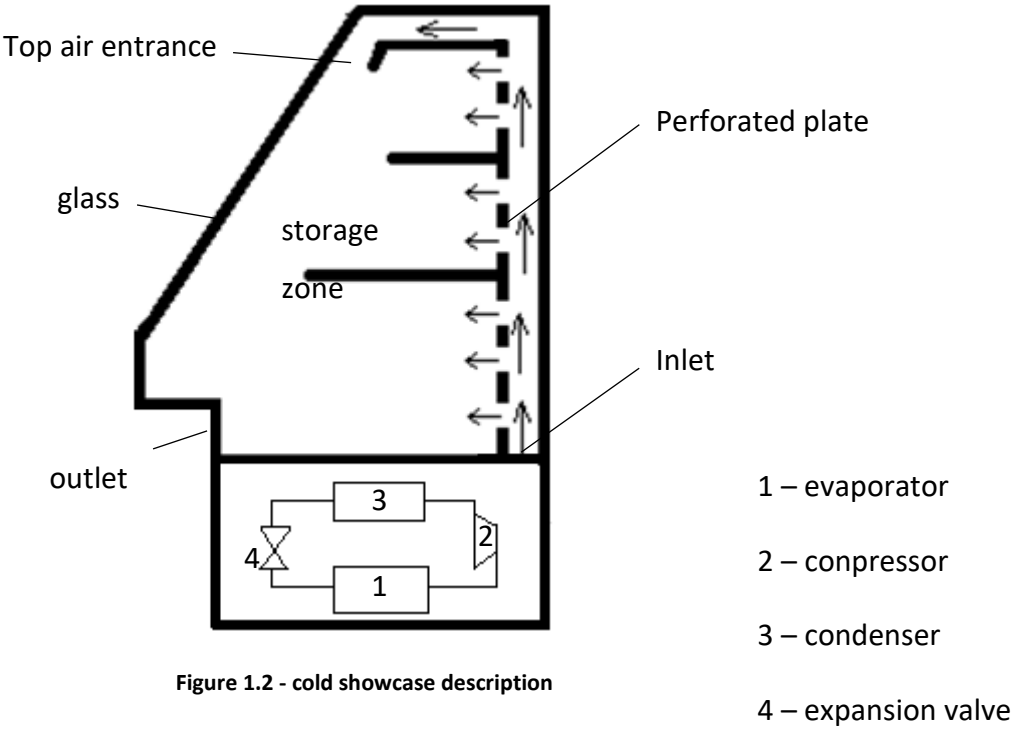

Figure 1.2 - cold showcase description

Air enters the storage area through the back of the showcase (through a perforated plate) and through an existing channel on the top. Afterwards, the air is exhausted from the bottom of the storage zone, entering the cold production zone again, starting a new cycle. The existence of a perforated plate is crucial to ensure uniformity of flow in the storage zone. This area is bounded by a glass on the face that is customer-facing because the glass is a transparent material to facilitate customer choice. If there is a freezing zone, it is not visible, and it is attached to the cold production zone.

It is also common that in the storage zone there are different temperatures intended for different foods, even in equipment without freezing.

1.2. Objectives

As referred before, the main goal is to optimize the showcase in order to reduce its consumptions without compromising its purpose. There are 2 methods to evaluate this kind of situations: computational and experimental. The computational method is an extension of the mathematical, but its faster and it is easier to visualise the problem. The main reason for using CFD as a tool to optimize the equipment is the reduced cost

and time when compared to experimental studies. So, the project should follow this schedule:

- Modelling a closed display cabinet
- Study of the flow in a closed display cabinet in order to determine the following parameters:

- The temperature range inside it, so that this range of values is the smallest possible and that these temperatures allow the preservation of food.
- The flow velocity so that it does not exceed a certain value (so that it does not produce excessive noise and does not dehydrate the food)
- Study the influence of different parameters and the relative importance of each one.
- Influence of the heat flux from all sources, namely heat transfer from the exterior through the boundaries and dissipated power from electric devices (for example the lamps).
- Influence of the products in the refrigerating process.

1.3. Dissertation structure

Considering the objectives mentioned before, in the next chapter the problem will be contextualized, explaining the origin of the cold air entering the storage zone. Some classifications of this type of equipment will be presented according to different entities, and finally a brief literature review including CFD and experimental work.

Chapter 3 will introduce numerical simulation and the software ANSYS-Fluent used for this project, considering some calculation strategies included on it and its functionalities.

In chapter 4, the case study will be presented, including the geometry, mesh definition and mesh optimization. It will be explained how to optimize the mesh to the study.

In chapter 5, the influence of several parameters will be studied. The last case studied will include products, for which a new geometry and mesh will be needed. For each model, there will be a small explanation of why this model was made and the next step of the study.

Finally, the last chapter will draw some conclusions and propose some future work that can continue this research.

2. STATE OF ART

In this chapter, the problem will be described, and the equipment will be presented and its working process. Then it will be presented the legislation to this kind of equipment and its classification considering the properties and operation parameters. Lastly, some scientific papers and other works similar to this one will be reviewed.

Figure 2.1 presents the full showcase, with the cold production zone and the storage zone.

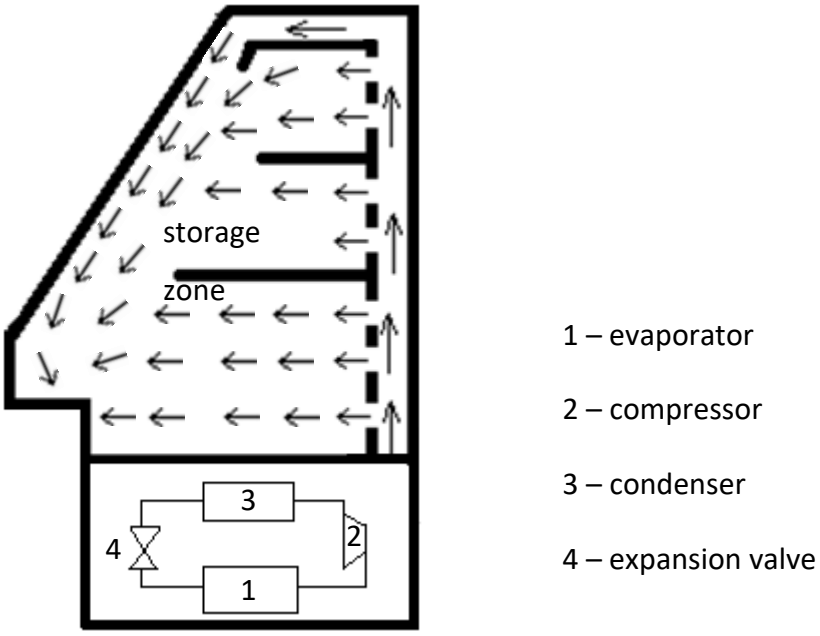

Figure 2.1 - showcase's full scheme, including the cold production zone and the storage zone

The next subchapter explains how the cold is produced in this kind of equipment. However, in the present study, this process will be ignored and it will be considered only the storage zone.

2.1. Problem description

The most common system used in the showcases to produce cold is by vapour compression (figure 2.2)

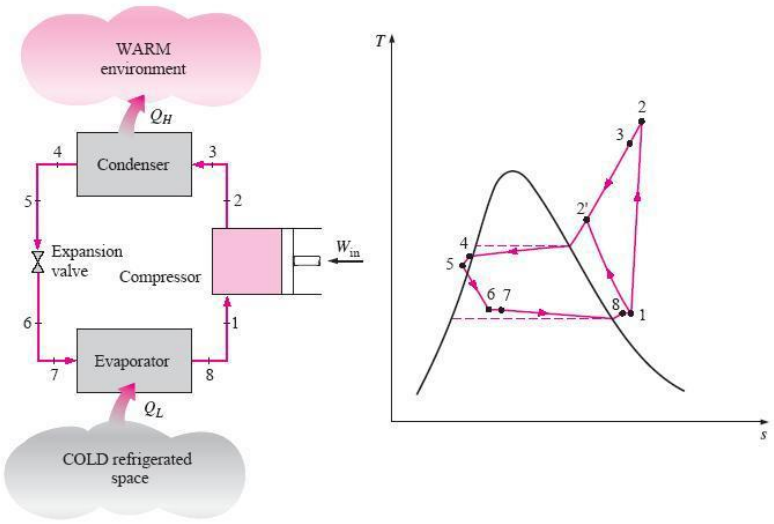

Figure 2.2 – Real steam compression system[2]

At point 1, the refrigerant is in a state of superheated vapour (in an ideal cycle, it would be saturated steam, but in the real case it is not to guarantee that there is no liquid in the compressor). Then there is a compression in order to raise the temperature and pressure of the refrigerant before the condenser, which will remove heat from the fluid. At this stage, the energy from the refrigerant can/should be used to warm the environment or another process in order to monetize all the energy (most important step of the heat pump). The refrigerant at the end of the condenser is liquid (similarly the liquid is subcooled to guarantee there is no gas on the expansion). Then there is an expansion valve before the refrigerant enters in the evaporator when it will be heated by the refrigerated space, restarting another cycle. This refrigerated space will be the study object of this project.

There are many other systems used in certain situations that will not be analysed because they are not relevant in this case[3].

Therefore, the main goal of this project is the improvement of the efficiency in a showcase, that is reducing the consumptions without compromising its purpose. The consumption reduction is achieved by lowering the mass flow rate and/or increasing the air inlet temperature (reducing the power of the refrigeration system). In order to optimize the equipment, the temperature field will be evaluated inside the showcase, maintaining the inlet conditions.

2.2. Cold equipment classification

Thus, several classifications were assigned according to their application and operating parameters. According to the European Community PRODCOM (from the French 'PRODuction COMmunautaire'), the cold store can be fitted in the code 'CPA 29.23.13: Refrigerating and freezing equipment (table 2.1) and heat pumps, except household type equipment', which can be divided into several subgroups [4]:

Table 2.1 - Classification of refrigerating equipment according to PRODCOM

Code	Description	Characteristics
29.23.13.33	Refrigerated show-cases and counters incorporating a refrigerating unit or evaporator for frozen food storage	Refrigerated and frozen food
29.23.13.35	Refrigerated show-cases and counters incorporating a refrigerating unit or evaporator (excluding for frozen food storage)	Refrigerated good
29.23.13.40	Deep-freezing refrigerating furniture (excluding chest freezers of a capacity ≤ 800 litres, upright freezers of a capacity ≤ 900 litres)	Frozen food, small equipment

29.23.13.50	Refrigerating furniture (excluding for deep-freezing, show-cases and counters incorporating a refrigerating unit or evaporator)	Frozen food, large equipment
29.23.13.90	Other refrigerating and freezing equipment	

The equipment under analysis is a commercial showcase that does not contain frozen food storage, so, considering this classification, this furniture fits in group 29.23.13.35.

There are many other entities using other classifications, such as EUROVENT, US Department of Energy, Energy Star Program requirements, etc. that are more precise, considering the following specifications:

- Volume
- Operating temperature:
  - Refrigeration (temperature higher than 0°C)
  - Freezing (temperature bellow 0°C)
  - Combined refrigeration and freezing
- Vertical or horizontal
- Self-contained or remote compression
- With or without doors, material (solid doors or glass)
- Opening type: sliding or pivoting.

The normative EN ISO 23953 classifies equipment according to their orientation (vertical, semi-vertical or horizontal), shape (line-up, islands, etc), operating temperature, service type (self-service or assisted service).

2.3. Literature review

Ribeiro et al (2016) [5] developed a numerical study (2D) using 3 different models of an open vertical display cabinet: the first one using a simple air curtain, the second one using deflection blades and the third one using multiples air curtains. These curtains

are refrigerated by the evaporator on the bottom. The air velocity was defined at the exit of the evaporator. This study surprisingly obtained better results on the first model (figure 2.3); however, it refers that the second one has more potential if the deflection blades were optimized. According to the author, the third model was not successful because of the increment of complexity. These results have natural limitations due to being performed in 2D simulations.

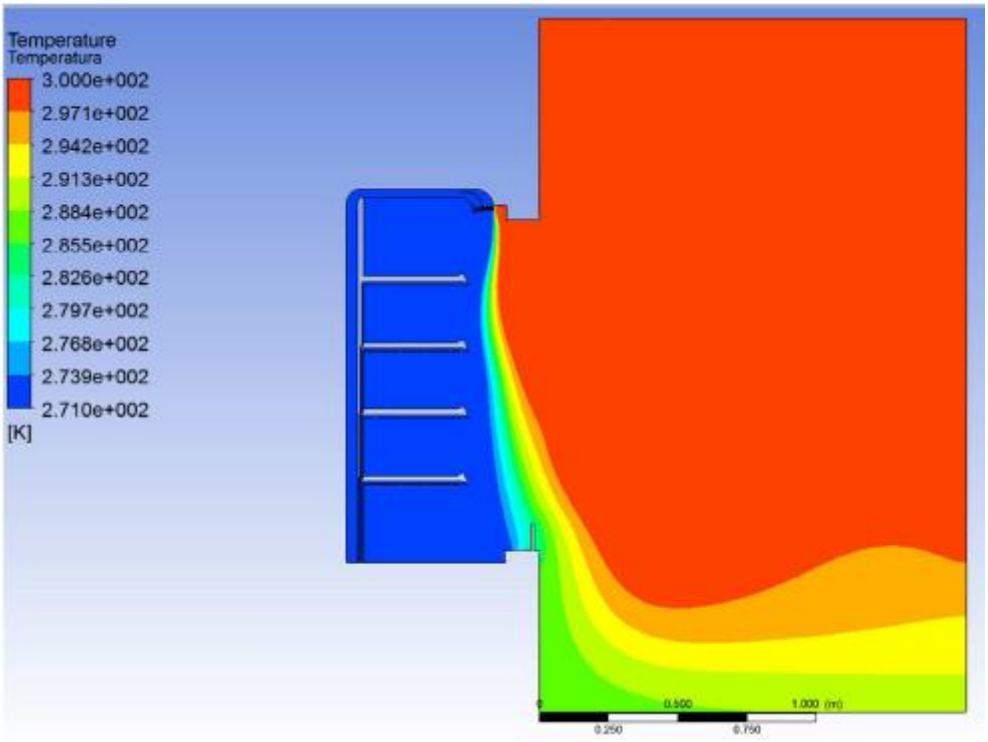

Figure 2.3 - Temperature field using multiple air curtains[5]

Chaomuang et al. (2019) developed an experimental study of a closed display cabinet, where the main goals were analysing the factors that influence the temperature inside the equipment and its variation, comparing these results with the same cabinet but with the doors opened (figure 2.4) [6]. The authors observed that 70% of the heat transfer was due to thermal bridges and gaps (for example the air infiltration between the doors). Comparing the temperatures with and without doors (when the cabinet was empty), in the storage zone there was an increment from 0.4 to 3.1°C and from 8.2 to 9.5°C in the shelf edges (near the air curtain). The influence of ambient temperature was

also studied: the authors verified that there is an almost linear relationship between the air temperature inside the equipment and the external temperature.

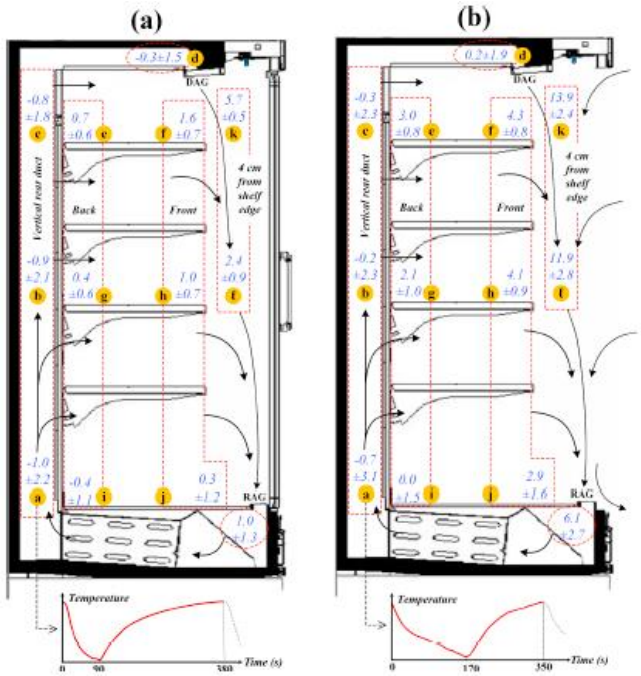

Figure 2.4 - mean temperature and standard deviations of the display cabinet with doors (a) and without doors (b), [6]

Wang et al. (2015) developed a numerical 3D study of an iced drink refrigeration cabinet, where the temperatures inside fluctuate between -7°C and -5°C, using an automated switch on and automated switch off [7].

The cabinet has an enclosing perforated plate that separates the evaporator and the storage room, which is simulated by the porous jump model. In the coolant air chamber, there is a fan in the bottom to assist the air circulation (figure 2.5).

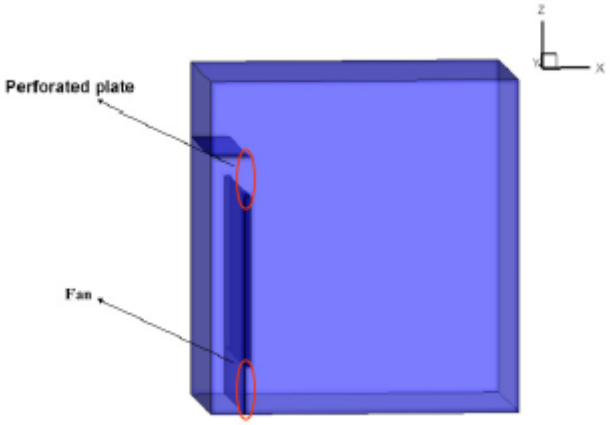

Figure 2.5 - Iced drink cabinet description, (Wang et al., 2016)

The first time the switch turns on, the refrigeration cabinet is at the same temperature of the room, 25°C. The switch remains on until the temperature reaches the lower limit, -7°C (first stage). Then the switch turns off and the temperature inside the cabinet will naturally raise due to the room temperature being higher until the temperature is -5°C (second stage), when the switch turns on, starting a new cycle (third stage). The authors conclude that in order to obtain satisfying results they had to simulate the full process (figure 2.6).

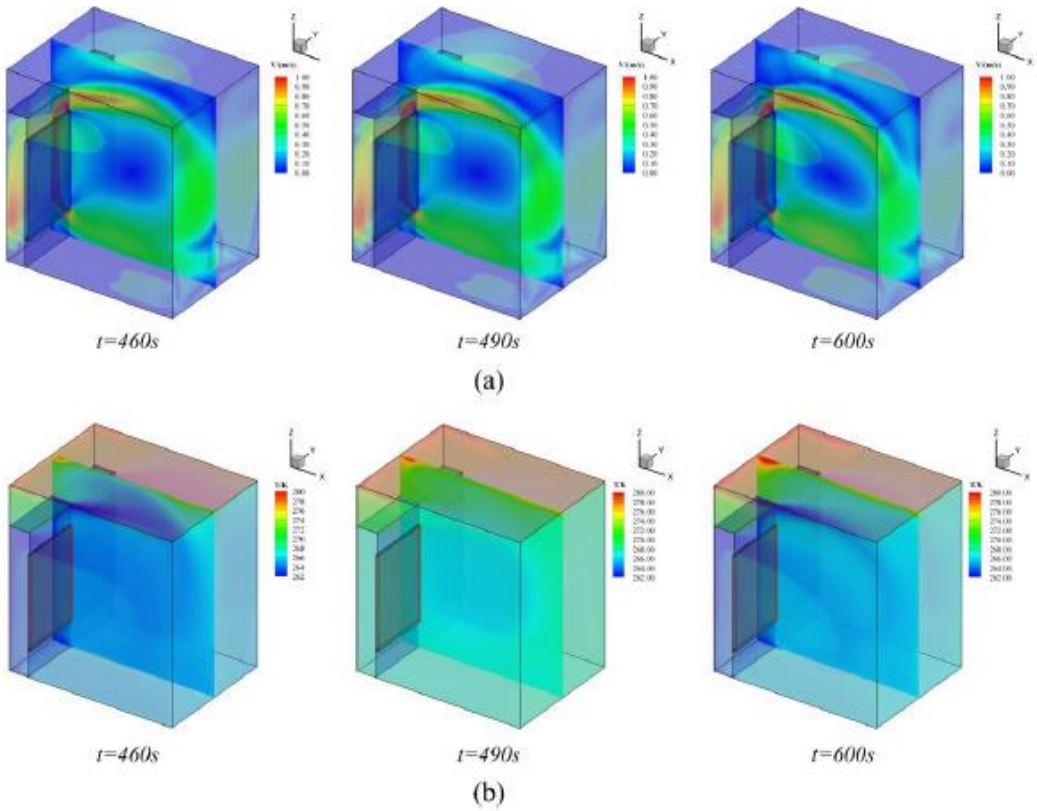

Figure 2.6 - results at the end of each stage: (a) flow field, (b) temperature field, [7]

Belman-Flores et al. (2016) built up a numerical study in order to analyse the temperature and flow in a refrigerator [8]. Its dimensions are 0.4m × 0.35m × 0.50m (width, depth, height) and use three different fluids for the cooling system: ammonia, water and hydrogen, which are the refrigerant, absorbent and auxiliary gas, respectively. The authors main objective was analysing the conditions on the compartment food storage (temperature and velocity) and compared it in different conditions, such as shelf position (top and bottom) and with or without finned surface (figure 2.7)

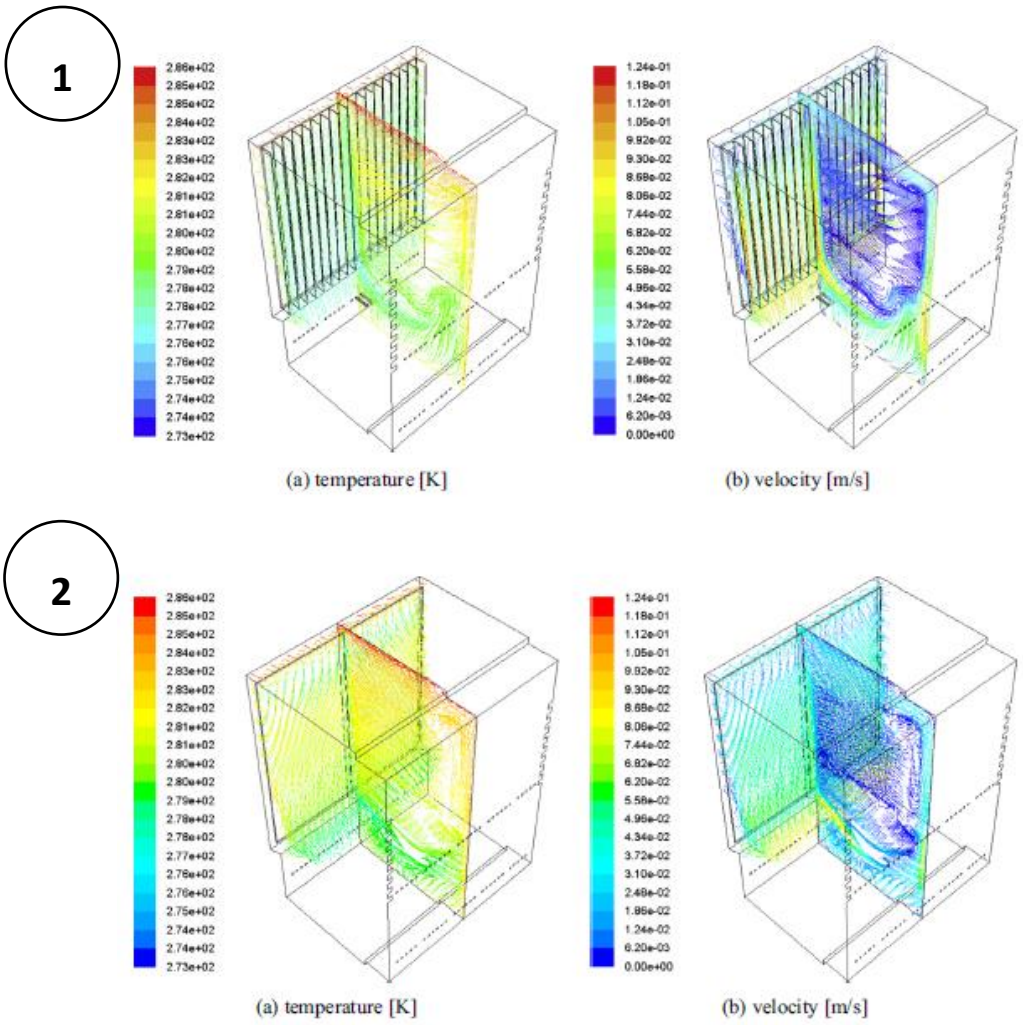

Figure 2.7 - Pathlines for plate evaporator, 1 - with a finned surface, 2 – without a finned surface, [8]

They concluded that there is a difference in the average temperature of 0.7K, which means that the model without a finned surface is an acceptable option. In terms of energy consumption, both models have similar results. This model can still have great improvements with an optimal geometry of the plate evaporator.

3. COMPUTATIONAL MODEL

Fluid flows are governed by partial differential equations that represent the laws of conservation of mass, *momentum* and energy. CFD includes fluid mechanics, numerical analysis and computational science, transforming the partial differential equations into systems of algebraic equations with solution algorithms that calculate the value of the desired variables.

The computational analysis can be divided into 3 components: pre-processing, solver and post-processing. Pre-processing involves all the preparation and conditions definition needed for the calculation, such as geometry, mesh and boundary conditions. Solver includes the calculation of all variables intended for the study. On post-processing, the results are analysed in many different ways, such as contours, vector graphics, video, etc.

Pre-Processing

At this stage, the physical problem is defined by adapting itself to the treatment of the solver. Pre-Processing is divided into the following phases:

- Geometry and problem's domain definition;
- Mesh creation is the division of the geometry in control volumes;
- Selection of physical phenomenon to study.
- Definition of fluid properties and boundary conditions

The solution of the problem is defined on the nodes in the interior of each control volume since the precision of the solution is directly related to the refinement of the mesh. That is if a mesh is refined the result of the simulations for greater accuracy. However, there is a maximum accuracy that can be achieved, so the mesh should be optimized in order to save computational time. The control volume should be as small as possible in areas where there is a more abrupt change in flow properties while in areas where there is no such change in fluid properties the volume of the control may already be larger (for example: in the simulation of the laminar flow of a fluid in a pipeline the mesh must be more refined next to the walls of the pipeline since it is in

that zone where there will be a greater variation of the flow rate, whereas when approaching the axis of the pipeline the mesh does not need to be so refined).

Solver

In Fluent there are two numerical methods based on the finite volume technique: pressure-based and density-based solver. The first is used for problems in which the flows are incompressible and at low speed while the second one is more suitable for studies of compressible flow and high speed. In both cases, the velocity value is given by the momentum equation. In the first method, the density is obtained through the equation of continuity, while the other method the solution of the pressure field is given by the manipulation of the equation of continuity with the momentum equation.

Both methods follow these steps:

- Initially, the previously defined mesh is divided into discrete control volumes.
- Integration of the equations into each control volume, thus constructing the discrete algebraic equations of dependent variables (the ones to be calculated), such as velocity, temperature, pressure, and so on.
- Linearization of the discretized equations and solution resulting from the system of linear equations of the dependent variables.

Post-processing

ANSYS Fluent Software has a wide range of graphic capabilities in the post-processing interface, including:

- Visualization of geometry and mesh;
- Vector graphics;
- Coloured contours and flow lines
- Particles trajectory;
- Images manipulation;
- Possibility of creating video files simulating the fluid flow.

3.1. Mathematical model

The main equations of the mathematical model are the mass conservation law, continuity and energy equation:

Mass conservation law (continuity equation)

This law is based on the mass balance in the element, that means that the mass variation in the control volume is equal to the net change in mass in the control volume.

The net change is the difference between the mass entering each face is the same as that which exits on the opposite side of that control volume. So, the mass variation in the control volume is given by:

$$\frac{\partial}{\partial t}(\rho\delta x\delta y\delta z) = \frac{\partial \rho}{\partial t}(\delta x\delta y\delta z) \qquad 3.1$$

In turn, the mass passing through each face of the control volume is given by the product of the density and the velocity in the component normal to the face of the control. Let u, v and w be the velocities along the x, y, and z axes respectively. Figure 3.1 shows the mass flows in the control volume, which is given by:

$$\begin{aligned}&\left(\rho u - \frac{\partial \rho u}{\partial x}\frac{1}{2}\partial x\right)\delta y\delta z - \left(\rho u - \frac{\partial \rho u}{\partial x}\frac{1}{2}\partial x\right)\delta y\delta z \\ &+ \left(\rho v - \frac{\partial \rho v}{\partial y}\frac{1}{2}\partial y\right)\delta x\delta z - \left(\rho v - \frac{\partial \rho v}{\partial y}\frac{1}{2}\partial y\right)\delta x\delta z \\ &+ \left(\rho w - \frac{\partial \rho w}{\partial z}\frac{1}{2}\partial z\right)\delta x\delta y - \left(\rho w - \frac{\partial \rho w}{\partial z}\frac{1}{2}\partial z\right)\delta x\delta y\end{aligned} \qquad 3.2$$

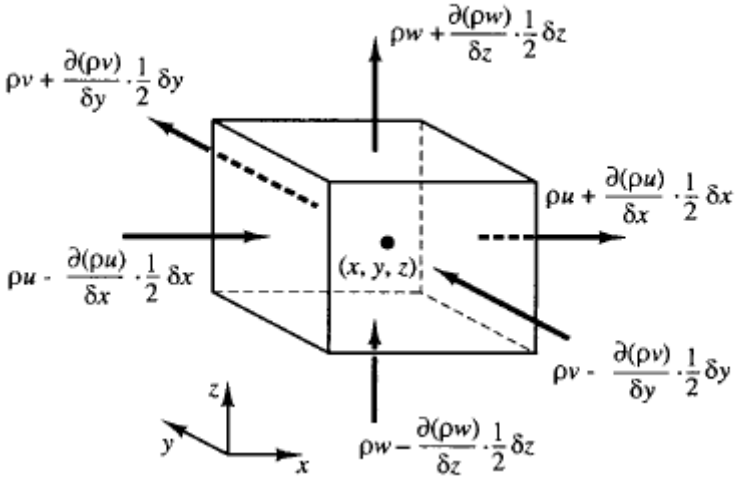

Figure 3.1 - Continuity on control volume, [9]

Adding the transient term and dividing all terms by δxδyδz:

$$\frac{\partial \rho}{\partial t} + \frac{\partial \rho u}{\partial x} + \frac{\partial \rho v}{\partial y} + \frac{\partial \rho w}{\partial z} = 0 \qquad 3.3$$

The last equation represents the mass conservation of three-dimensional transient flow in a compressible fluid. The first term represents the term transient while the others represent the term convective

Momentum conservation law (momentum equation)

According to Newton's 2nd law *F = ma*, the momentum in the control volume particle is equal to the sum of the forces in the particle. The variation of momentum in the x, y, and z axes per unit volume in the control volume is given by:

$$\rho \frac{Du}{Dt} \; in \; x \; ; \; \rho \frac{Dv}{Dt} \; in \; y; \; \rho \frac{Dw}{Dt} \; in \; z \qquad 3.4$$

There are two types of forces in the control volume:

- **Surface forces**
  - Forces due to pressure
  - Forces due to viscosity

- **Body forces**
  - Forces due to gravity
  - Centrifugal forces
  - Coriolis forces
  - Electromagnetic forces

Surface forces will be considered in terms of momentum and the body forces contained in the source term.

In a three-dimensional case, the stress state in the fluid element is defined in terms of pressure and nine components of viscosity stresses as shown in Figure 3.2. The pressure is identified by the letter *p* and the viscous stress by the letter *τ*.

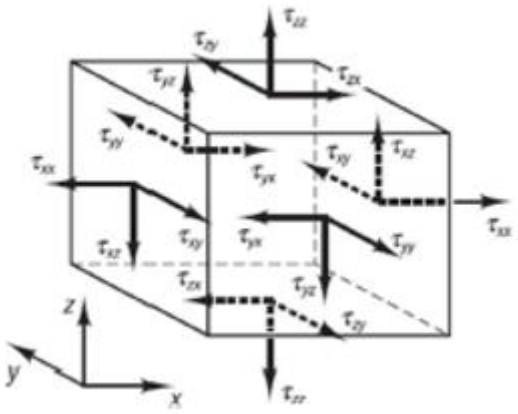

Figure 3.2 - Conservation of momentum, [9]

Considering that the forces on the components in *x* resulting from the pressure *p* and the surface stresses *τxx*, *τxy* and *τxz*, (Figure 3.3). The resulting force in x is the sum of all the components acting in that direction of the element.

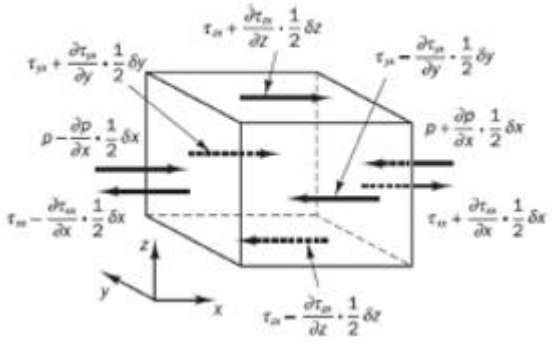

Figure 3.3 - Conservation of momentum in x, [9]

The resulting forces in x on the faces (E, W) are:

$$\begin{aligned}&\left[\left(p-\frac{\partial p}{\partial x}\frac{1}{2}\delta x\right)-\left(\tau_{xx}-\frac{\partial \tau_{xx}}{\partial x}\frac{1}{2}\delta x\right)\right]\delta y\delta z\\&+\left[-\left(p-\frac{\partial p}{\partial x}\frac{1}{2}\delta x\right)-\left(\tau_{xx}-\frac{\partial \tau_{xx}}{\partial x}\frac{1}{2}\delta x\right)\right]\delta y\delta z\\&=\left(-\frac{\partial p}{\partial x}+\frac{\partial \tau_{xx}}{\partial x}\right)\delta x\delta y\delta z\end{aligned} \qquad 3.5$$

In faces (N, S) in the x-axis results:

$$-\left(\tau_{yx}-\frac{\partial \tau_{yx}}{\partial y}\frac{1}{2}\delta y\right)\delta x\delta z+\left(\tau_{yx}-\frac{\partial \tau_{yx}}{\partial y}\frac{1}{2}\delta y\right)\delta x\delta z=\frac{\partial \tau_{yx}}{\partial y}\delta x\delta y\delta z \qquad 3.6$$

Lastly, the forces on direction x on faces (T, B) are given by:

$$-\left(\tau_{zx}-\frac{\partial \tau_{zx}}{\partial z}\frac{1}{2}\delta z\right)\delta x\delta y+\left(\tau_{zx}-\frac{\partial \tau_{yx}}{\partial z}\frac{1}{2}\delta z\right)\delta x\delta y=\frac{\partial \tau_{zx}}{\partial z}\delta x\delta y\delta z \qquad 3.7$$

The total force by volume unit of the fluid resulting from the surface tensions is obtained by the sum of equations mentioned above, which divided by δxδyδz results:

$$\frac{\partial(-p+\tau_{xx})}{\partial x}+\frac{\partial \tau_{yx}}{\partial y}+\frac{\partial \tau_{zx}}{\partial z} \qquad 3.8$$

The equation of momentum in component x is obtained by the equality of the momentum variation with the resultant of the force due to the surface tensions of the equation (previous equation) plus the term source in x.

$$\rho\frac{Du}{Dt}=\frac{\partial(-p+\tau_{xx})}{\partial x}+\frac{\partial \tau_{yx}}{\partial y}+\frac{\partial \tau_{zx}}{\partial z}+SMx \qquad 3.9$$

Similarly, on the y component:

$$\rho\frac{Dv}{Dt}=\frac{\partial(-p+\tau_{yy})}{\partial y}+\frac{\partial \tau_{yx}}{\partial x}+\frac{\partial \tau_{zy}}{\partial z}+SMy \qquad 3.10$$

And z component:

$$\rho\frac{Dw}{Dt}=\frac{\partial(-p+\tau_{zz})}{\partial z}+\frac{\partial \tau_{yz}}{\partial y}+\frac{\partial \tau_{zx}}{\partial x}+SMz \qquad 3.11$$

Energy conservation law (Energy equation)

This equation is derived from the first law of thermodynamics which states that the internal rate of change of a fluid particle is the sum of the variation of heat and the variation of the work.

Saying that the variation rate ρ is given by:

$$\rho\frac{DE}{Dt} \qquad 3.12$$

Work is equal to the product of force by the component of velocity in the direction of the force. Making the product of equation 3.9 with the velocity in the component in x:

$$\frac{\partial u(-p+\tau_{xx})}{\partial x}+\frac{\partial(u\tau_{yx})}{\partial y}+\frac{\partial(u\tau_{zx})}{\partial z} \qquad 3.13$$

The same happens with y and z components, obtaining respectively:

$$\frac{\partial v(-p+\tau_{yy})}{\partial y}+\frac{\partial(v\tau_{xy})}{\partial x}+\frac{\partial(v\tau_{zy})}{\partial z} \qquad 3.14$$

$$\frac{\partial w(-p+\tau_{zz})}{\partial z}+\frac{\partial(w\tau_{yz})}{\partial y}+\frac{\partial(w\tau_{xz})}{\partial x} \qquad 3.15$$

Isolating the terms that contain pressure p:

$$-\frac{\partial(up)}{\partial x}-\frac{\partial(vp)}{\partial y}+\frac{\partial(wp)}{\partial z}=-div(pu) \qquad 3.16$$

The total work variation resulting from the superficial forces is given by:

$$\begin{aligned}&[-div(pu)]+\left[\frac{\partial(u\tau_{xx})}{\partial x}+\frac{\partial(u\tau_{yx})}{\partial y}+\frac{\partial(u\tau_{zx})}{\partial z}\right]\\&+\left[\frac{\partial(v\tau_{xy})}{\partial x}+\frac{\partial(v\tau_{yy})}{\partial y}+\frac{\partial(v\tau_{zy})}{\partial z}\right]\\&+\left[\frac{\partial(w\tau_{xz})}{\partial x}+\frac{\partial(w\tau_{yz})}{\partial y}+\frac{\partial(w\tau_{zz})}{\partial z}\right]\end{aligned} \qquad 3.17$$

Equation 3.17 represents the balance of all x, y, and z components of work on the fluid particle resulting from forces acting on surfaces.

The balance of the heat flux through the faces of the control volume is represented by the vector of heat flow q in the three components q_x, q_y and q_z, according to Figure 3.4.

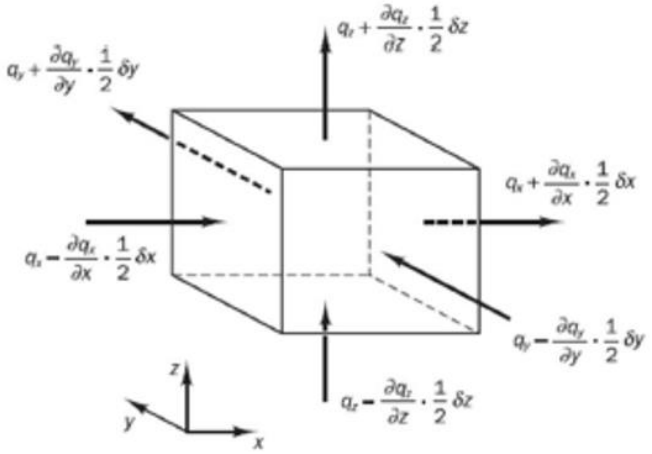

Figure 3.4 - Energy conservation,[9]

$$\left[\left(q_x - \frac{\partial q_x}{\partial x}\frac{1}{2}\delta x\right) - \left(q_x + \frac{\partial q_x}{\partial x}\frac{1}{2}\delta x\right)\right]\delta y \delta z = -\frac{\partial q_x}{\partial x}\delta x \delta y \delta z \qquad 3.18$$

The same happens for the components y and z.

$$-\frac{\partial q_y}{\partial y}\delta x \delta y \delta z \qquad 3.19$$

$$-\frac{\partial q_z}{\partial z}\delta x \delta y \delta z \qquad 3.20$$

Dividing the equations above by *δxδyδz:*

$$-\frac{\partial q_x}{\partial x} - \frac{\partial q_y}{\partial y} - \frac{\partial q_z}{\partial z} = -div\ q \qquad 3.21$$

According to the Fourier law for the heat flow by conduction:

$$q_x - K\frac{\partial T}{\partial x};\ q_y - K\frac{\partial T}{\partial y}; q_z - K\frac{\partial T}{\partial z} \qquad 3.22$$

That can be expressed by:

$$q = -k grad\ T \qquad 3.23$$

Combining the two previous equations, the final energy balance equation is obtained resulting from the conduction heat transfer process.

$$-div\ q = div\ (k\ grad\ T) \qquad 3.24$$

3.2. Turbulence models

Most flows studies are turbulent studies. A flow is defined as laminar, intermediate or turbulent through the Reynolds number. This number is given by the ratio of inertial forces to viscous forces (UL / v). Since U is the velocity of the fluid, L is the characteristic length of the flow, and v is the kinematic viscosity. For low values of the Reynolds number the flow is laminar, above the critical value (transient Reynolds value) the flow becomes turbulent.

The ANSYS fluent software uses an approach to the numerical simulation names RANS (Reynolds Averaged Navier-Strokes Simulation) [10]. This technique solves time-averaged Navier-Strokes equations and offers several methods of turbulence for all turbulent length. This is the most common approach in the industry due to his low cost compared to other ones (DNS, LES). There are many turbulent models that can be used in this approach, which must be chosen considering the Reynolds number, fluid properties and its application (Table 3.1).

Table 3.1 - Turbulence models description

Model	Behaviour and usage
Spalart-Allmaras	Economical for large meshes. Performs poorly for 3D flows, free shear flows, flows with strong separation. Suitable for mindly complex (quasi-2D) external/internal flows and boundary layer flows under pressure gradient (e.g. airfoils, wing, airplane fuselages, missiles, ship hulls
Standard k- ε	Robust. Widely used despite the known limitations of the model. Performs poorly for complex flows involving severe pressure gradient, separation, strong streamline curvature. Suitable for initial screening or alternative designs, and parametric studies
Realizable k- ε	Suitable for complex shear flows involving rapid strain, moderate swirl, vortices, and locally transitional flows (e.g. boundary layer separation, massive separation and vortex shedding behind bluff bodies, stall in wide-angle diffusers, room ventilation).
RNG k- ε	Offers largely the same benefits and has similar applications as Realizable. Possibly harder to converge than realizable.
Standard k- ω	Superior performance for wall-bounded boundary layer, free shear, and low Reynolds number flows. Suitable for complex boundary layer flows under adverse pressure gradient and separation (external aerodynamics and turbomachinery). Can be used for transitional flows (thought tends to predict early transition). Separation is typically predicted to be excessive early
SST k- ω	Offers similar benefits as standard k- ω. Dependency on wall distance makes this less suitable for free shear flows.

RSM	Physically the most sound RANS model. Avoids isotropic eddy viscosity assumption. More CPU time and memory required. Tougher to converge due to close coupling of equations. Suitable for complex 3D flows with strong streamline curvature, strong swirl/rotation (e.g. curved duct, rotating flow passages, swirl combustors with very large inlet swirl, cyclones).

There will be studied two different models, Realizable k-ε and SST k-ω, which can be the most suitable for this study and its variations.

Turbulence model Realizable k-ε (RKE)

This model, like the Standard k-ε (SKE) model, is suitable for most situations but has some benefits compared to the previous one, such as:

• Accurately predicts the spreading rate of both planar and round jets.

• Also, likely to provide superior performance for flows involving rotation, boundary layers under strong adverse pressure gradients, separation, and recirculation.

It is expected to have some rotation in this case study, that is the main reason the SKE was excluded for this situation.

Turbulence model SST k-ω

k-ω models have better performance for boundary layer flows and low Reynolds number flows. SST k-ω specifically, is a mix of a k-ω model near the wall and k-ε in the freestream (Figure 3.6).

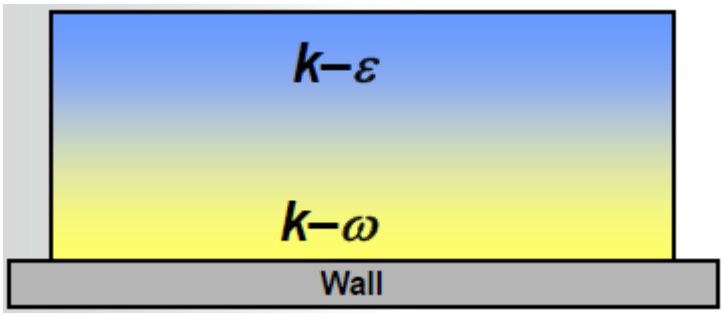

Figure 3.5 – SST k-ω model definition[10]

This model is a good compromise between k-ω and k-ε models.

Near wall treatment

Four different models can be chosen in order to define the flow behaviour near the wall: Standard wall functions, Non-equilibrium wall functions, Enhanced wall treatment, User-Defined Wall functions.

As it was done in the turbulence models, standard wall functions and enhanced wall treatment models will be considered.

Standard wall functions model is designed for high Re attached flow, the near-wall region is not resolved, the near-wall mesh is relatively coarse.

The enhanced wall treatment model is used for low Re flows or flows with near-wall complex phenomena. Usually requires a very-fine near-wall mesh capable of resolving this region but can also handle coarse near-wall mesh.

3.3. Finite volumes

The finite volume method uses as a starting point the integral form of the conservation equation.

The domain of the solution is divided into a number of control volumes, the above equation is applied to each of them (Figure 3.7). At the central point of each volume control is located a computational node, in which the values of the desired variables are calculated, as it happens in the boundaries of the volume control. The values of the variables at the boundary are obtained through interpolations as a function of nodal values (in the centre).

Volume and surface integrals are approximated using appropriate quadrature formulas. As a consequence, an algebraic equation is obtained for each volume control, in which the value of the variable to be studied appears in this node and in the neighbours. This method can be used in any type of mesh, so it can be used in very complex geometries. The mesh itself defines all the boundaries of the volume control; however, it does not need to be related to the coordinate system. This method is

conservative, provided that the surface integrals are shared on each face of the volume and control.

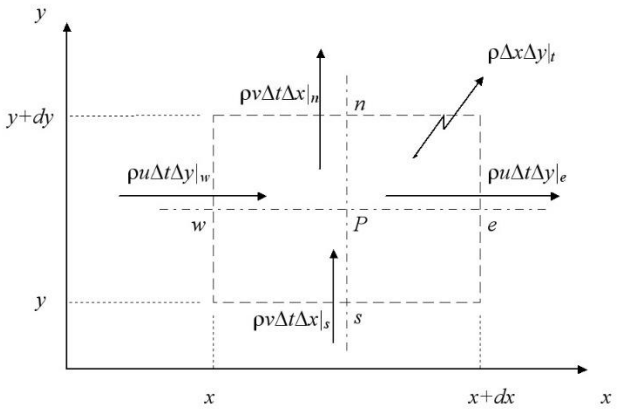

Figure 3.6 -Fluxes in a 2D element according to finite volumes method, [9]

Momentum equation

If the pressure field is known, the discretization of the velocity equations and the resolution is identical to a scalar equation. For this analysis, a new notation will be used. The nodes will be named with uppercase letters and vectors with lowercase letters. Consider a node P: This node is located on the coordinates I, J, then the one that is next to it on the right (E) is located on the coordinates I, J+1 and the vector that connect these nodes is $u_{I+1,\ J}$. Following the same logic, the point immediately above (N) is in the coordinates I + 1, J and vector that connect these nodes is $v_{I,\ J+1.}$

Figure 3.8 illustrates a mesh with the designations of the various nodes and vectors

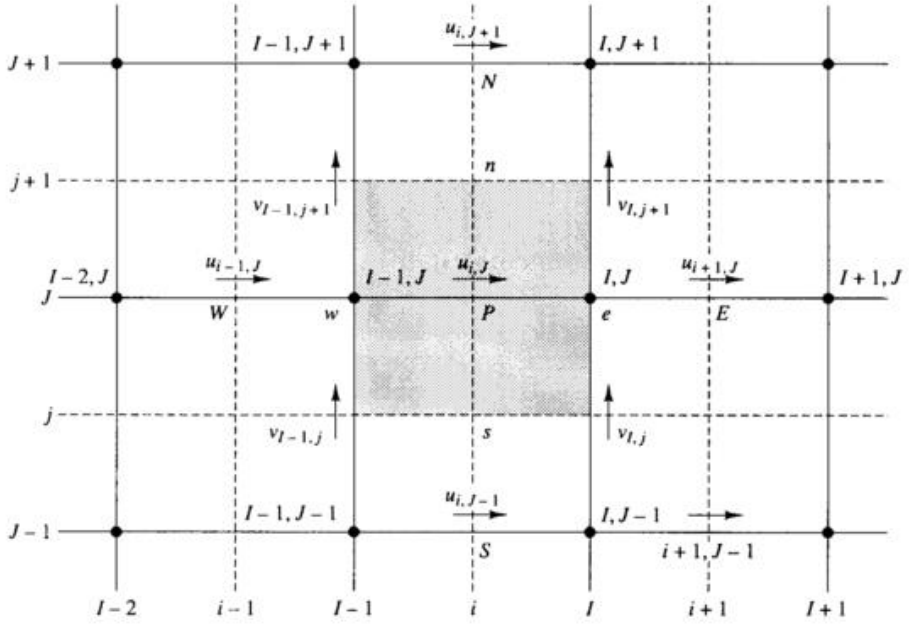

Figure 3.7 - Nodes and vector designation in a 2D element according to finite volumes method, [9]

The momentum equations (u,v) with this new coordinate system are given by:

$$a_{i,J}u_{i,J} = \sum a_{nb}u_{nb} + (p_{I-1,J} - p_{I,J})A_{i,J} + b_{i,J} \qquad 3.26$$

$$a_{i,J}v_{I,j} = \sum a_{nb}v_{nb} + (p_{I,J-1} - p_{I,J})A_{i,J} + b_{i,J} \qquad 3.27$$

3.4. SIMPLE

The acronym SIMPLE means "Semi-Implicit Method Pressure-Linked Equations". The initial algorithm consisted basically of an attempt/error methodology in calculating the pressure in the elements. This method was developed considering a 2D stationary laminar flow using Cartesian coordinates.

To start the calculation according to this algorithm, the value of **p*** is arbitrated. The momentum equations are discretized and solved in order to **u*** and **v***

$$a_{i,J}u^*_{i,J} = \sum a_{nb}u^*_{nb} + \left(p^*_{I-1,J} - p^*_{I,J}\right)A_{i,J} + b_{i,J} \qquad 3.28$$

$$a_{i,J}v^{*}{}_{I,j} = \sum a_{nb}v^{*}{}_{nb} + \left(p^{*}{}_{I,J-1} - p^{*}{}_{I,J}\right)A_{i,J} + b_{i,J} \quad 3.29$$

The difference between the actual pressure and the pressure estimated can be defined by **p'**. Using this logic for **u** and **v**, the actual values of pressure and velocities is obtained by the following equations:

$$\begin{aligned} p &= p* + p' \\ u &= u* + u' \\ v &= v* + v' \end{aligned} \quad 3.30$$

Equations (3.28) and (3.29) will be used substituting the values estimated by the differences defined above:

$$a_{i,J}u^{*}{}_{i,J} = \sum a_{nb}u'{}_{nb} + \left(p'{}_{I-1,J} - p'{}_{I,J}\right)A_{i,J} + b_{i,J} \quad 3.31$$

$$a_{i,J}v^{*}{}_{I,j} = \sum a_{nb}v'{}_{nb} + \left(p'{}_{I,J-1} - p'{}_{I,J}\right)A_{i,J} + b_{i,J} \quad 3.32$$

From this moment an approximation will be made: $\sum a_{nb}u'{}_{nb}$ e $\sum a_{nb}v'{}_{nb}$ will be considered equal to zero. The omission of this plot is the main error associated with the SIMPLE method. Therefore:

$$u'{}_{i,J} = d_{i,J}(p'{}_{I-1,J} - p'{}_{I,J})A_{I,J} \quad 3.33$$

$$v'{}_{I,j} = d_{I,j}(p'{}_{I,J-1} - p'{}_{I,J})A_{I,J} \quad 3.34$$

$$\text{where } d_{i,J} = \frac{A_{i,J}}{a_{i,J}} \text{ e } d_{J,i} = \frac{A_{I,j}}{a_{I,j}} \quad 3.35$$

Combining the equations (3.31) to (3.35), it results:

$$u_{i,J} = u^*_{i,J} + d_{i,J}(p'_{I-1,J} - p'_{I,J}) \quad 3.36$$

$$v_{I,j} = v^*_{I,j} + d_{I,j}(p'_{I,J-1} - p'_{I,J}) \quad 3.37$$

The same logic can be applied to $u_{i+1,J}$ e $v^*_{I,j}$.

Until now only the momentum equations was considered but the velocity field should also satisfy the continuity equation. The continuity is satisfied discretely for the scaled control volume shown in Figure 3.9:

$$[(\rho uA)_{i+1,J} - (\rho uA)_{i,J}] + [(\rho vA)_{I,j+1} - (\rho vA)_{I,j}] = 0 \quad 3.38$$

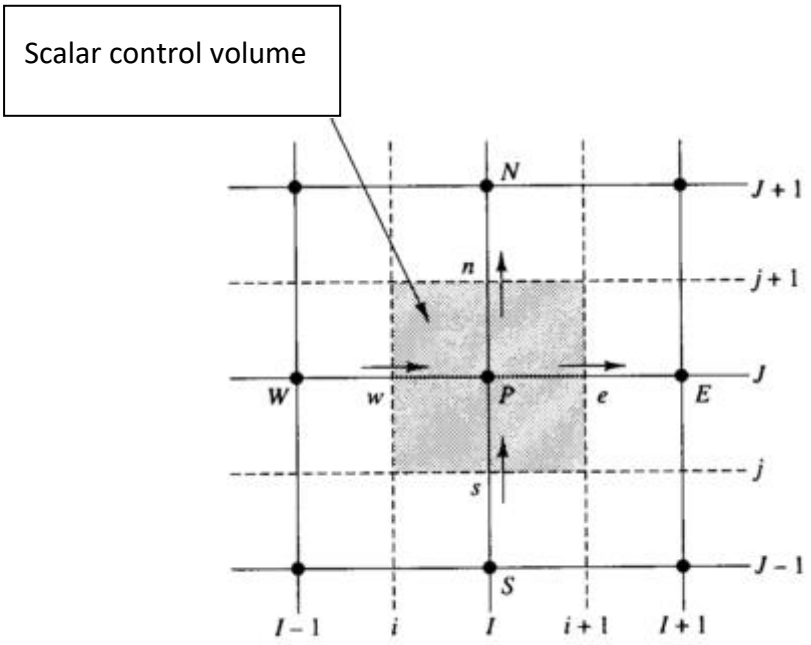

Figure 3.8 - Control volume, [7]

The velocity-corrected values of equations are substituted and rearranged in equations (3.36) and (2.37) in the discretized continuity equation. In order to simplify the equation, the coefficients presented in Table 1 were created.

$$a_{I,J}p'_{I,J} = a_{I+1,J}p'_{I+1,J} + a_{I+1,J}p'_{I+1,J} + a_{I,J+1}p'_{I,J+1} + a_{I,J-1}p'_{I,J-1} + b'_{I,J} \quad 3.39$$

where $a_{I,J} = a_{I+1,J} + a_{I-1,J} + a_{I,J+1} + a_{I,J-1}$ and the coefficients are the following:

Table 3.2 - Coefficients definition

$a_{I+1,J}$	$a_{I-1,J}$	$a_{I,J+1}$	$a_{I,J-1}$	$b'_{I,J}$
$(\rho dA)_{i+1,J}$	$(\rho dA)_{i,J}$	$(\rho dA)_{i,J+1}$	$(\rho dA)_{i,J}$	$(\rho u^* A)_{i,J}-(\rho u^* A)_{i+1,J}+(\rho v^* A)_{I,j}-(\rho v^* A)_{I,j+1}$

Equation (3.39) represents the discretized continuity equation as an equation for the pressure correction p'. The term source b' in the equation is the perturbation of continuity resulting from the incorrect velocity field u* and v*. Solving equation (3.39), the pressure correction p 'can be obtained for all points. Once these values are known, the actual pressure field must be obtained using equation (3.30) and the velocity components through equations (3.36) and (3.37). The omission of terms $\sum a_{nb}u'_{nb}$ e $\sum a_{nb}v'_{nb}$ in the derivation does not affect the final solution because the pressure and velocity corrections are zero in a convergent solution given by p^*=p, u^*=u, v^*=v.

The pressure equation correction is susceptible to divergence unless some under-relaxation factor is used during the iterative process and better pressure values are obtained with:

$$p^{new} = p^* + \alpha_p p', \quad 3.40$$

where α_p is the under-relaxation factor. If the relaxation factor equal to one, the estimated pressure field is corrected by p'. However, the corrections p', in particular when the estimated field p* is far from the final solution, is often too large for stable simulations. A value of α_p equal to one does not apply correction, which also makes no sense. Therefore, choosing a value between 0 and 1 allows us to add to the pressure

field p* a fraction of the pressure p' that is large enough to proceed with the iterative process, but small enough to have stable simulations.

The velocity values are also under-relaxed. The variation of velocity components is given by:

$$u^{new} = \alpha_u u + (1 - \alpha_u) u^{n-1}$$
$$v = \alpha_v v + (1 - \alpha_v) v^{n-1} \qquad 3.41$$

Those factors α_u *e* α_v are relaxation factors of the components of velocities u and v, comprised between 0 and 1, and u^{n-1} e v^{n-1} represent the velocity values obtained in the previous iteration.

The equation of pressure correction is also affected by the sub-relaxed velocity and it can be shown that the terms *d* of the pressure correction are as follows

$$d_{i,J} = \frac{A_{i,J}\alpha_u}{a_{i,J}}, \quad d_{i+1,J} = \frac{A_{i+1,J}\alpha_u}{a_{i+1,J}}, \qquad d_{I,j} = \frac{A_{I,j}\alpha_v}{a_{I,j}} \quad \text{and} \quad d_{I,j+1} = \frac{A_{I,j+1}\alpha_v}{a_{I,j+1}} \qquad 3.42$$

The coefficients in denominator refer to the positions (i, J), (i + 1, J), (I, j) and (I, j + 1) of a scalar cell referring to point P.

A correct choice of sub-relaxation factors is essential for a good cost/efficiency ratio of the simulations. Too high a value can cause oscillations in the solution or even divergent solutions, on the other hand very low values imply a higher computational cost. Unfortunately, there is no optimal value, this value depends on the flow and this value must be optimized in each case.

3.5. Residual values and convergence

At the end of each iteration, the residuals of continuity, momentum and energy are calculated and saved, thus creating a history of convergence. After the discretization, the conservation equation of any dependent property is given by the following equation:

$$a_p \emptyset_p = \sum_{nb} a_{nb} \emptyset_{nb} + b \qquad 3.43$$

Where a_p is the coefficient of the centre of the control volume, a_{nb} the contribution of the neighbouring cell coefficients and *b* the contribution of the constant to the source term.

$$a_p = \sum_{nb} a_{nb} - S_p \qquad 3.44$$

The calculated value of the residual by software according to the Pressure-based model is given by the unbalance of equation (3.42) summed in all cells, this is a non-staggered residue and is written as follows:

$$R^{\emptyset} = \sum_{cells\ P} \left| \sum_{nb} a_{nb} \emptyset_{nb} + b - a_p \emptyset_p \right| \qquad 3.45$$

The software uses two models of staggered residues, representative of the flow Ø through the domain. These are global scaling and local scaling. They are respectively defined by the following equations:

$$R^{\emptyset} = \frac{\sum_{cells\ P} \left| \sum_{nb} a_{nb} \emptyset_{nb} + b - a_p \emptyset_p \right|}{\sum_{cells\ P} \left| a_p \emptyset_p \right|} \qquad 3.46$$

$$R_{\emptyset} = \frac{\sqrt{\sum_{cells}^{n} (\frac{1}{n})} \left(\frac{\sum_{nb} a_{nb} \emptyset_{nb} + b - a_p \emptyset_p}{a_p} \right)^2}{(\emptyset_{max} - \emptyset_{min})_{domain}} \qquad 3.47$$

Residual values are a good indicator of the convergence of problems. By default, ANSYS Fluent activates the global scaling option. There are some models to evaluate the

convergence of results. The definition of residual values in some cases is sufficient to ensure convergence but may be misleading in other cases. It is, therefore, good practice to assess convergence not only by the value of residues but also by monitoring some specifications, such as the heat transfer coefficient. Figure 3.10 shows the configuration panel of the residuals, and in the image, the values of the residuals were assigned by default by the program.

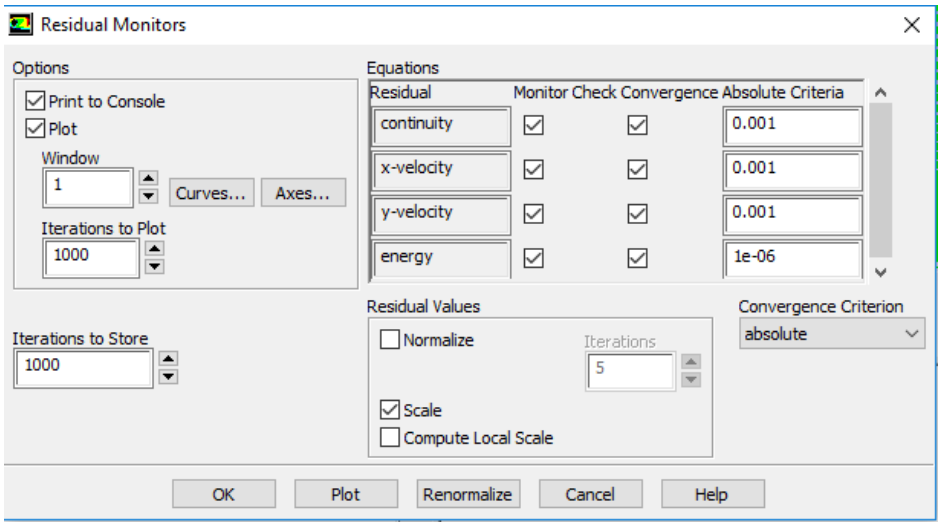

Figure 3.9 - Residual values definition on ANSYS - FLUENT

4. CASE STUDY

In this chapter, the main strategies adopted in the study are presented. The physical parameters, geometry and mesh are presented as well as the optimization of the mesh

4.1. Strategies adopted

Analysing this type of equipment, it can be realized that the initial geometry is very simple. The first models are tests that do not include some conditions of the last models. As the simulations go on, these conditions will be considered one by one until the final model is accomplished. This strategy allows us to detect errors and their origins and correct them before the final model is accomplished. The last simulations include products which will transpose in more complex geometry.

The first decision to make is choosing between a 2D or a 3D geometry. Showcases usually have a transversal section that is uniform, so the 3D geometry would probably not accomplish better results compared with the 2D, but the complexity and the computational resources would be much higher. For these reasons, this study would be focused on a 2D geometry (figure 4.1)

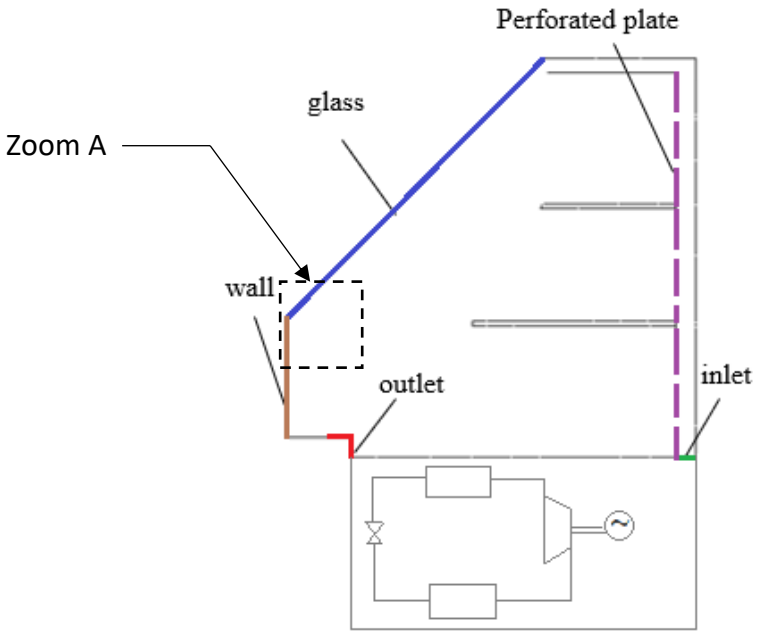

Figure 4.1 - Showcase's geometry with no products in the shelves

The first concern is to approximate the geometry to reality and simplify it whenever is possible without compromise the reliability of the results. With that said, a velocity inlet will be considered, with air at 0°C and ignore the cold production zone, focusing only on the storage zone.

However, some care is needed when transposing the real geometry to 2D because there are some details that cannot be perfectly represented in a 2D geometry. In this showcase is not possible to design the air entrances as they are, because the lateral section is not constant in all the equipment. In the showcase the air intakes are holes but, in this geometry, they will be represented by a line, which means a rectangular rip at the full length. In order to not compromise the results and simplify the geometry, this line represents a rip that has the same area as the sum of the holes. The perforation area ratio (perforated area/total area) in the back is around 7.5%.

The first analysis after the geometry was defined was the mesh refinement. The simulation was started with a coarse mesh that would necessarily result in a bad solution. In the next simulations, the mesh was gradually thinner. At some point the solution does not depend on the mesh that was used, that means it is not necessary to refine more the mesh. In the next studies, a mesh that has roughly the same element size will be used.

Boundary conditions delimitate different zones of the domain. This limitation can be physical and easy to define, but sometimes the physical phenomenon is hard to translate in a boundary condition. Despite that, it is critical to have a boundary definition that has the best approach to reality in order to minimize the differences between the model and the reality.

Most of the boundary conditions were defined according to other experimental and numerical studies mentioned previously on the state of art in chapter 1.4.

In this case study different boundary conditions were used and also different initial values, which were optimized during the study:

- Inlet velocity = 2 m/s, according to other studies, the velocity is usually bellow 3m/s in order to reduce the noise. This value varies according to the refrigerated volume and inlet area[5], [11], [12].
- Pressure inlet = 0 Pa, the pressure on the equipment should be equal to the atmospheric pressure, this value is used by default on other studies similar to this one.
- Outlet: outflow, other studies may use pressure outlet but based on previous studies made for this showcase, outflow obtains better results[13].
- Inlet temperature = 0°C, the objective is to maintain the temperature at 5°C or lower in the product zone, but also higher than 0°C to avoid freezing. The inlet temperature is the lowest on the showcase because there are many heat sources during until the air reaches the outlet (environment temperature, products temperature, lamps, etc) and there are no temperatures below 0°C.
- Glass heat transfer: Q(glass) = 8.29 W/m^2, this value was used on previous studies for this showcase, but other values will be evaluated on further simulations[13].
- Initial temperature = 15^oC, this temperature should be equal to the temperature of the room where the showcase is, usually equal or lower than 25°C [12], [14].
- Turbulence model: RKE, according to the turbulence models available on the software (some of them analysed on chapter 3.2), this should be one of the most suitable models for room ventilation and standard situations like this one[10].

4.2. Mesh definition

Mesh consists in dividing the domain into small areas/volumes (in 2D or 3D simulations). In the 2D model were used only quadrangular elements. In order to accomplish a good mesh to further, the mesh definition was made in two steps. The first step was to choose the type of elements used (the choice was to use quadrilateral elements whenever is possible) and the size of each one related to the others. Smaller elements should be used in areas where stronger variations were expected. There are also some factors given by the program that were considered, like element quality,

minimum orthogonal quality, skewness, maximum aspect ratio and y+. These factors consider the element quality based on its shape (aspect ratio, orthogonal quality and skewness). The size variation between neighbour elements should also be verified. The element size variation should be smooth because of calculation stability. The simulation starts only after the mesh definition. The second step is to get the intended precision, this can be accomplished by using a coarse mesh (that may present low-quality results due to the low number of elements) and to increase the number of elements gradually. This raise of the number of the elements must be proportional in order to maintain a similar mesh between smaller elements, that way generates better results. At some point, as the number of elements were increased, the meshes start to converge and should present the same results regardless of the number of elements. The best mesh in this group is the one that has the least number of elements and presents the same results of all these with a higher number of elements. The showcase's geometry is presented in figure 4.2.

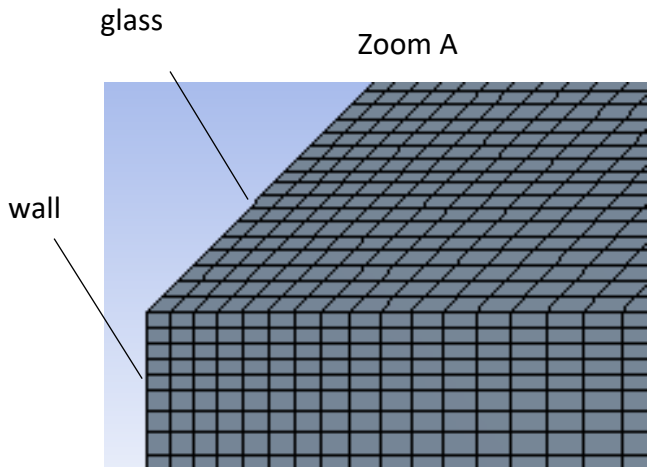

Figure 4.2 - Mesh definition near the glass and wall, element size = 1.65mm (mesh 4, approximately 230,000 elements)

As it is shown in figure 4.2 the elements that are closer to the wall are smaller because it is expected to have a higher variation of velocity in this area (boundary layer). This is because the air velocity close to the wall is zero (due to the friction) and quickly increases as moving away from the wall.

4.3. Mesh optimization

As mentioned in the last chapter, the first step is to optimize the mesh quality based on the factors given by the program. Some of these factors are presented in table 4.1.

Table 4.1 - Mesh quality report

Mesh number	Mesh report			
	Quality			Number of elements
	Average orthogonal quality	Average skewness	Average aspect ratio	
1	0.92	0.18	1.85	61225
2	0.92	0.18	1.98	93198
3	0.92	0.18	2.21	117247
4	0.93	0.17	2.18	232141
5	0.93	0.17	2.42	415295

Researching for a better mesh, some refinements were done based on the first mesh (mesh with 61,000 elements).

The second and third meshes (with 93,000 and 117,000 elements, respectively) were generated increasing the number of elements in all the domain, because the velocity results reveal some unexpected vortices (figure 4.4, meshes 1, 2) and was expected that the temperature variations were smoother (figure 4.3, meshes 1 and 2).

The fourth mesh (with 230,000) was created increasing the number of elements in all zones of the showcase because the temperature field still changed, despite the bigger changes were below the bottom shelf (figure 4.3, mesh 3). The velocity field remains similar, except bellow the top shelf the vortices generated are different (figure 4.4, mesh 3).

The fifth mesh (with 415,000 elements) was created increasing the number of elements in all the domain to confirm the results obtained for the fourth mesh (figures 4.3 and 4.4, meshes 4 and 5).

To the mesh study, there were used many different refinements, resulting in consecutively more elements: roughly 61,000 (mesh 1), 93,000 (mesh 2), 117,000 (mesh 3), 230,000 elements (mesh 4), 415,000 elements (mesh 5).

The lines in black represent the main streams of air.

The results in figure 4.3 and 4.4 represent 60 seconds in real-time for the temperature and velocity fields, respectively.

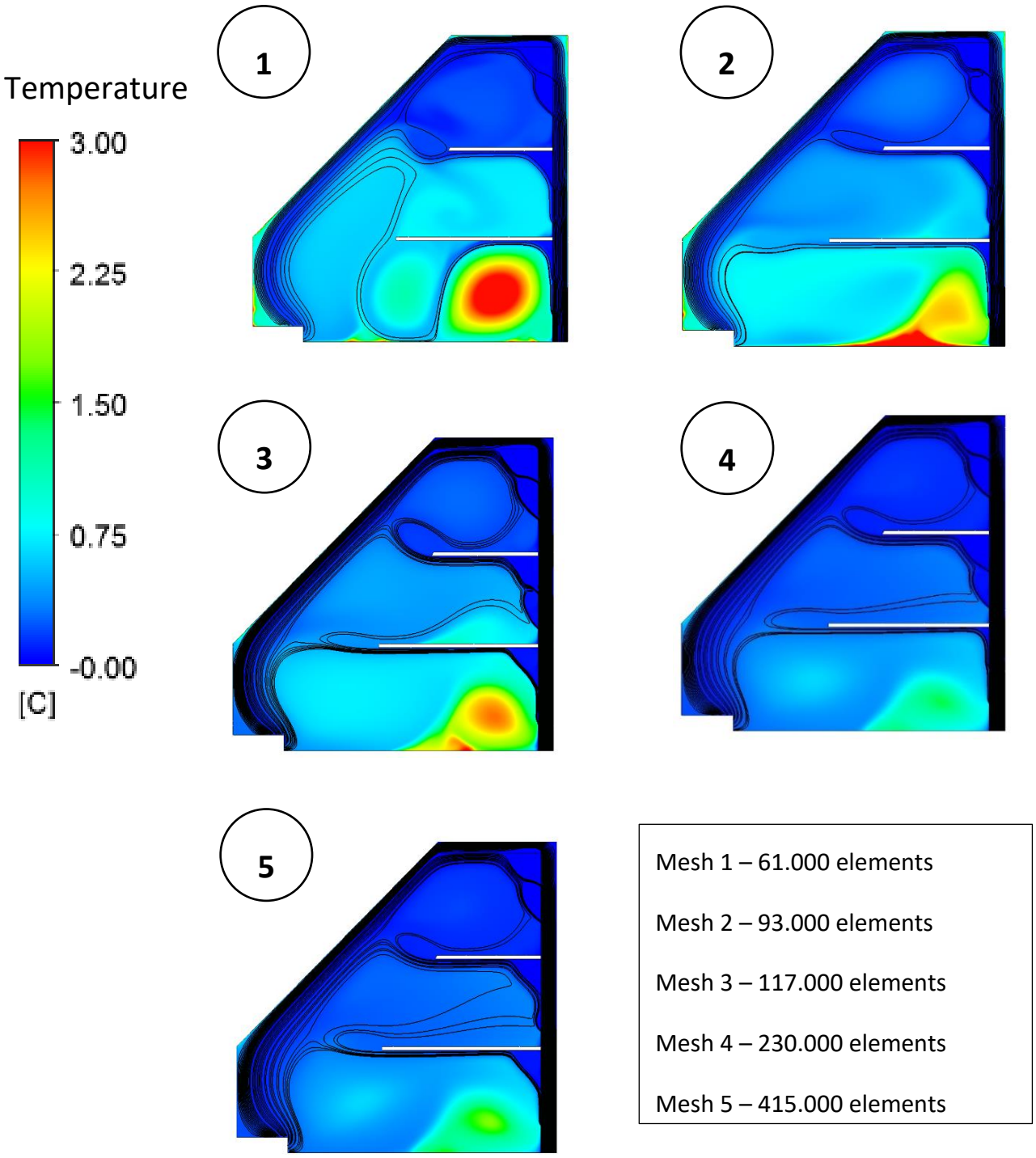

Figure 4.3 - Temperature field after 60s in the meshes 1 to 5, T_0 = 15ºC, v_0 = 2 m/s, T(inlet) = 0ºC, Q(glass) = 8.29 W/m²K

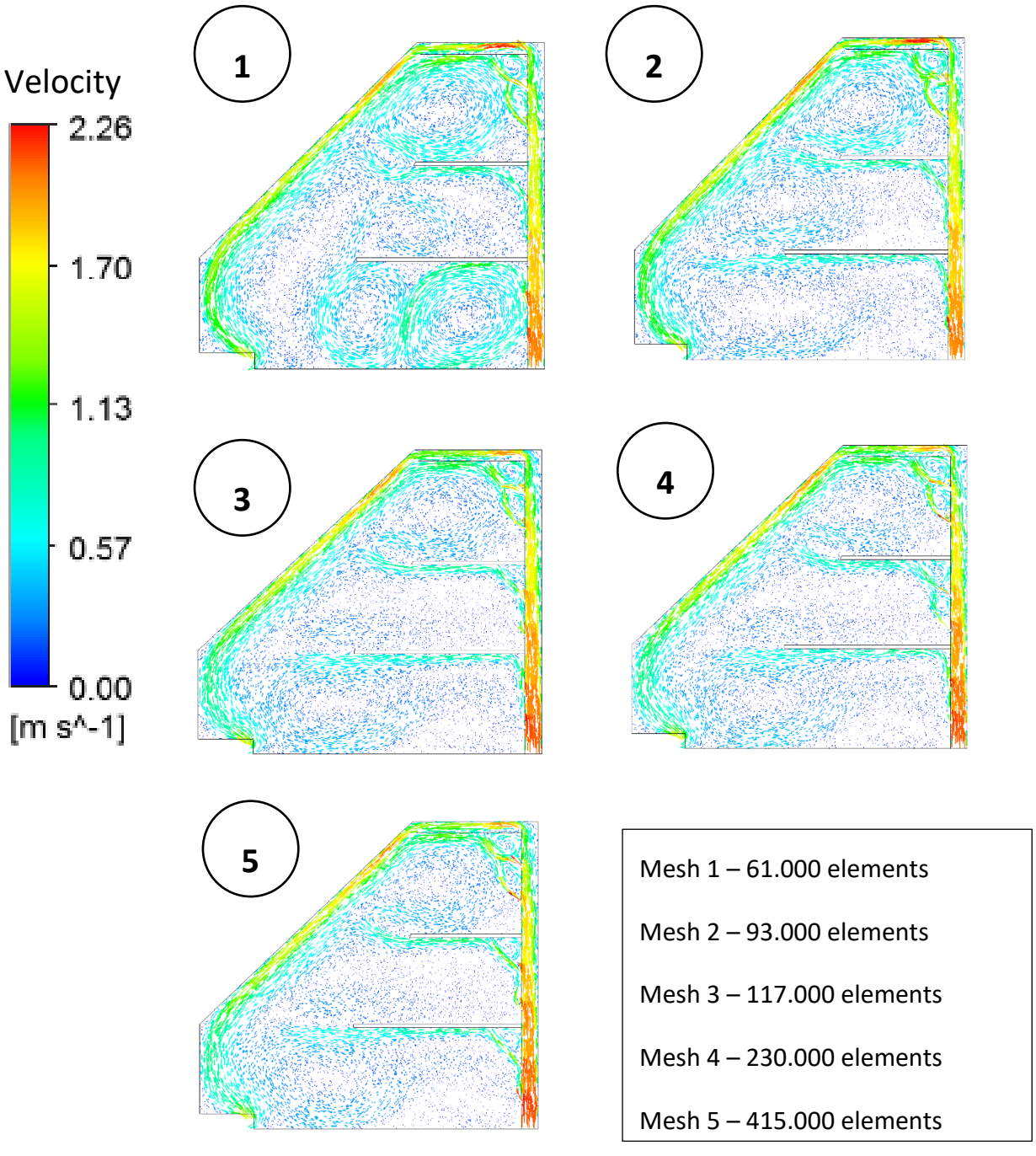

Figure 4.4 - Velocity field after 60s in the meshes 1 to 5, T_0 = 15ºC, v_0 = 2m/s, T(inlet) = 0ºC, Q(glass) = 8.29W/m²K

With the setup used in this simulation, it is expected that the temperature was below 5°C in all the domain, where the higher temperatures would be on the bottom because this area is the one that is farthest from the inlet, despite having small entrances on the back of the equipment. In the first and seconds meshes the number of elements is low, and two completely different results can be seen. The spots where the temperature is higher is different on both cases and there are too many vortices in the first mesh, so it can be concluded that these results are not correct due to the low number of elements. In the third mesh (approximately 117,000 elements), the results start to stabilize to a certain shape (figure 4.3, mesh 3), where there is a hot spot at the bottom due to the low-velocity values in this area, but it was not yet certain that this mesh was refined enough. So, at this stage, it was used two more meshes to confirm if the third one was refined enough, or the results were still susceptible to mesh variation

After analysing the results using meshes 4 and 5, it can be realized that there are still slight differences in temperatures between these two meshes and mesh 3 does not translate the same results that the last ones. Despite that, the results for the velocity values are closer, except on the back area, near the air entrances, where only on the most refined meshes it is possible to observe vortices. In this case, the velocity field remains the same, but the temperature distribution changes significantly, meaning there is still heat flux between the air inside the equipment and outside. Assuming that the flow may not be stationary yet, more simulations will be made until 120 seconds with meshes 4 and 5, instead of the 60 seconds used previously. It is also possible to verify that there is a hot spot on the bottom (figure 4.3), probably due to the fact that there is a dead zone, where the velocity is almost zero. Another aspect that can affect this phenomenon is the condition defined in the bottom wall. This condition is the same for all the walls, but this bottom boundary is very specific because it is the physical boundary between the refrigerated zone and the evaporator. Because of that, in future cases, other conditions will be studied in order to optimize the flow in this area.

Finally, analysing the temperature results obtained after 60 and 55 seconds (figure 4.6) it can be observed that the flow is not yet stationary, so for further simulations, the time will be 120 seconds.

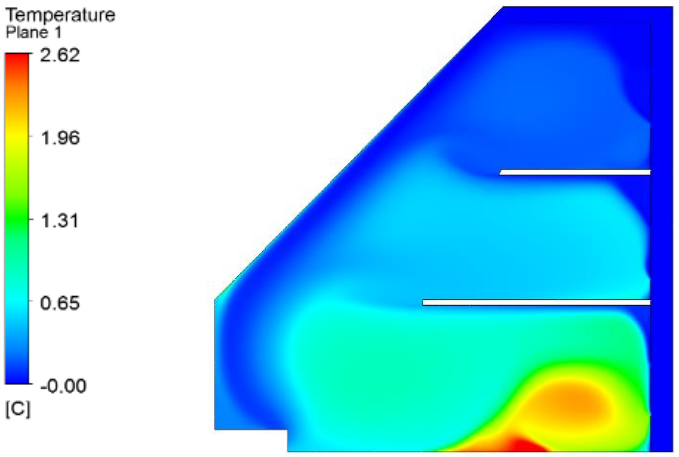

Figure 4.6 - temperature field for mesh 3 after 55 seconds, T_0 = 15°C, v_0 = 2m/s, T(inlet) = 0°C, Q(glass) = 8.29 W/m²K

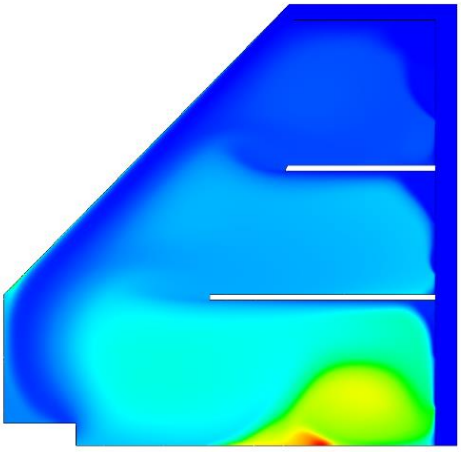

Figure 4.5 - temperature field for mesh 3 after 60 seconds, T_0 = 15°C, v_0 = 2 m/s, T(inlet) = 0°C, Q(glass) = 8.29 W/m²K

5. RESULTS AND DISCUSSION

This chapter will be divided into two groups: in the first one some boundary conditions will be considered/modified in the geometry/mesh previously defined:

- The temperature on the bottom wall, near the evaporator
- The heat flux through the glass
- The dimension of the holes on the perforated plate on the back

5.1. Study of some parameters influence

In chapter 4, many meshes were analysed in order to achieve the good mesh, with the desired precision and the minimum number of elements. However, in this analysis, only the basic parameters were introduced, such as velocity inlet, initial temperature, type of exit, etc. So, in this chapter other parameters will be studied one by one in order to perceive the influence of each parameter in the temperature and velocity fields.

5.1.1. Boundary condition on the bottom boundary: 0°C

It was decided that the further simulations would be done using 2 different meshes with the same refinement as meshes 4 and 5.

The objective is to develop the model in order to obtain results that may match the reality as better as possible. At this stage, the objective was to analyse the influence of the boundary conditions in the final results.

In the first simulations, a heat flow across the glass of 8.29 W/m^2 (figure 5.1) was used as a boundary condition. However, this value is affected by the temperatures inside and outside the showcase and the materials (glass, steel, etc), so the walls will have different boundary conditions depending on the conditions they are subject to.

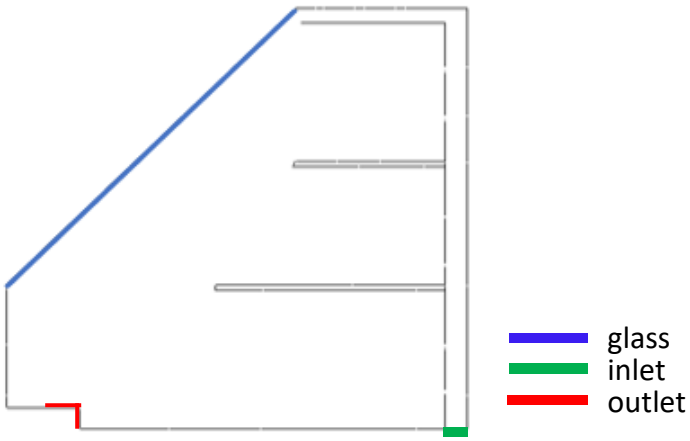

Figure 5.1 - definition of glass, inlet and outlet

The bottom boundary is very specific because below it is the evaporator. Due to this and despite the isolation, this wall should be colder than the other ones. For those reasons, the boundary condition used on this wall was a constant temperature of 0ºC (Tbottom = 0ºC). Figures 5.2 and 5.3 show the temperature and velocity field for these new conditions, respectively.

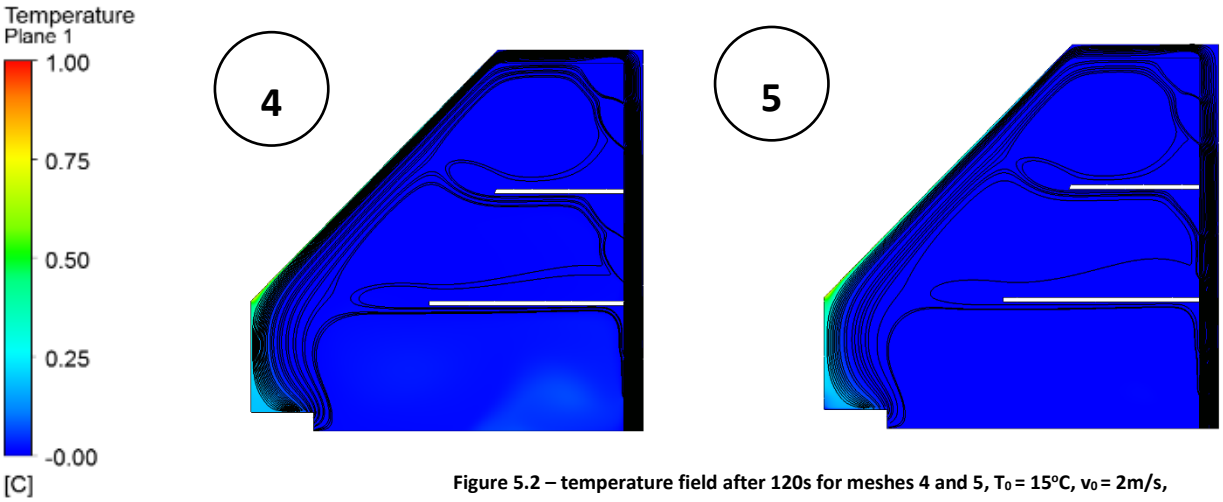

Figure 5.2 – temperature field after 120s for meshes 4 and 5, T_0 = 15ºC, v_0 = 2m/s, T(inlet) = 0ºC, Q(glass) = 8.29 W/m²K, T(bottom) = 0ºC

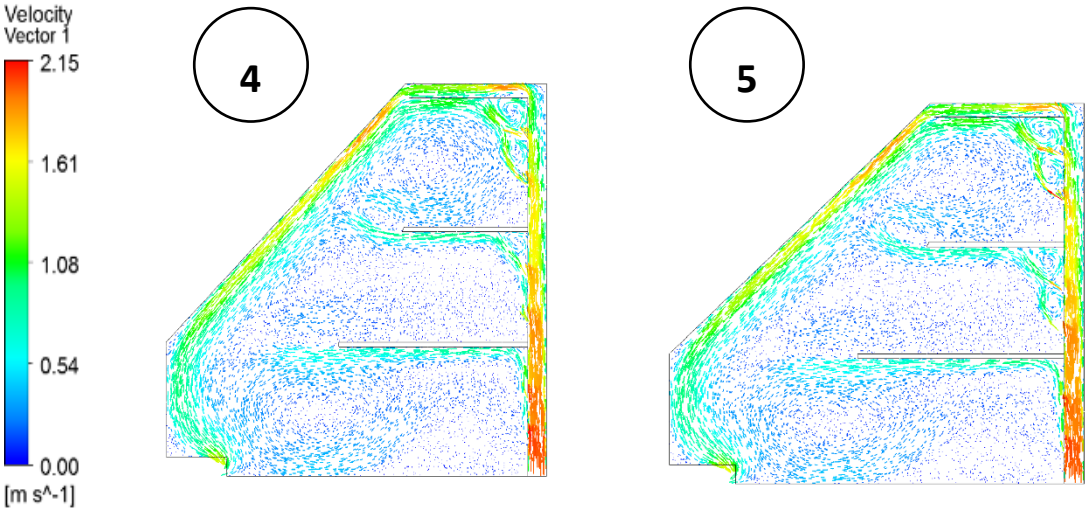

Figure 5.3 - velocity field after 120s for meshes 4 and 5, T_0 = 15°C, v_0 = 2 m/s, T(inlet) = 0°C, Q(glass) = 8.29 W/m²K, T(bottom) = 0°C

As expected, this new boundary condition lowered the air temperature in the display zone, but the velocity field remains similar. That is because the only parameter that was changed was the boundary temperature on the bottom wall, but the geometry and inlet conditions were maintained. There is also a big change due to the time changing, now the maximum temperature is less than 1°C. These values would be great, but at the same time, they are not real because not all the conditions were considered. So now it can be questioned that the heat transfer through the walls might be too low.

According to the bibliography, the heat transfer coefficient through the glass, U, may have different values depending on the type of glass it was used (simple, double glass, etc.). For simple glasses, the average U is 5,7 W/m^{2}K and for traditional double glasses U=2,8 W/m^{2}K [15]. Considering that the temperature differences between the air inside the equipment and the outside may be on average between 15 and 20°C, it can be concluded that the heat flux ($Q = U \times \Delta T$) is on average 42 W/m^2 for double glass and 114 W/m^2 for simple glass, which is considerably higher than the coefficient that was used on previous simulations.

With that said, in the next simulations some variations will be addressed in the heat flux values through the glass to 50 and 150 W/m^{2}K because of the uncertainty about these values.

5.1.2. Heat flux 50 and 150 W/m^{2}K

The following simulation was based on the same starting conditions as the previous one, varying only the heat flux defined through the glass.

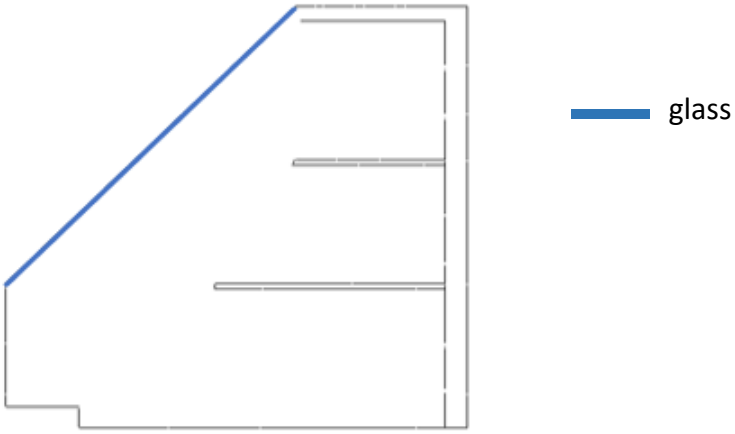

Figure 5.4 – glass boundary condition

For these simulations, new velocity fields will not be presented, because they are similar/equal to the previous ones. The figures 5.5 and 5.6 evidence the influence of heat transfer through the wall.

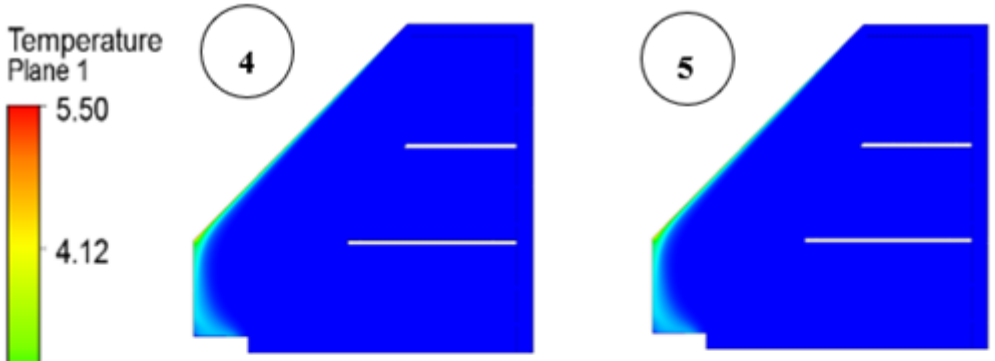

Figure 5.5 - temperature field after 120s, T_0=15ºC, v_0 = 2 m/s, T(inlet) = 0ºC, Q(glass) = 8.29 W/m²K, T(bottom) = 0ºC

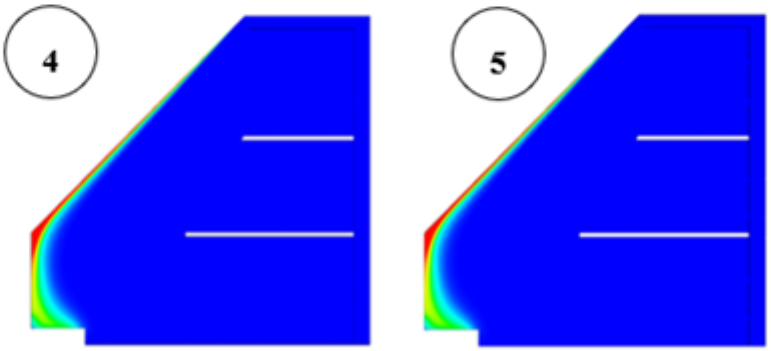

Figure 5.6 - temperature field after 120s, T_0 = 15ºC, v_0 = 2 m/s, T(inlet)=0ºC, Q(glass)=8.29 W/m²K, T(bottom) = 0ºC

As it can be seen on figures 5.5 and 5.6, the impact of this heat flux is only local for both 50 and 150 W/m^{2}K. The maximum temperature in the highest heat flux is not admissible. Although, as it can be seen in figure 5.6, those values only appear near the glass, which will not affect eventual products. Although the air curtain is at a higher temperature than the rest of the air inside the showcase, the hot air will be exhausted in a short period of time, preserving the conditions on the zone products. On the next simulations, the heat flux will be 50 W/m^{2}K.

5.1.3. Back entrances double size bottom

In previous simulations was evident that there was an issue below the bottom shelf because the velocity was too low, and that could cause some problems to the quality of the products, depending on which products are refrigerated. To avoid this, it was decided to increase the size of the holes in this zone in order to increase the mass flow (figures 5.7 and 5.8).

On this study, it was decided to use only mesh 4 because the previous simulations have the same results for mesh 4 and 5, so there is no point simulate with both meshes.

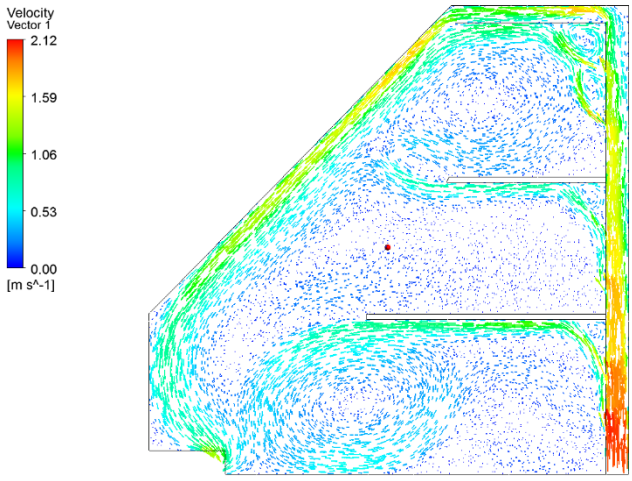

Figure 5.7 - velocity field after 120s, T_0 = 15ºC, v_0 = 2 m/s, T(inlet) = 0ºC, Q(glass) = 8.29 W/m²K, T(bottom) = 0ºC, with double sized entrances on the bottom of the perforated plate

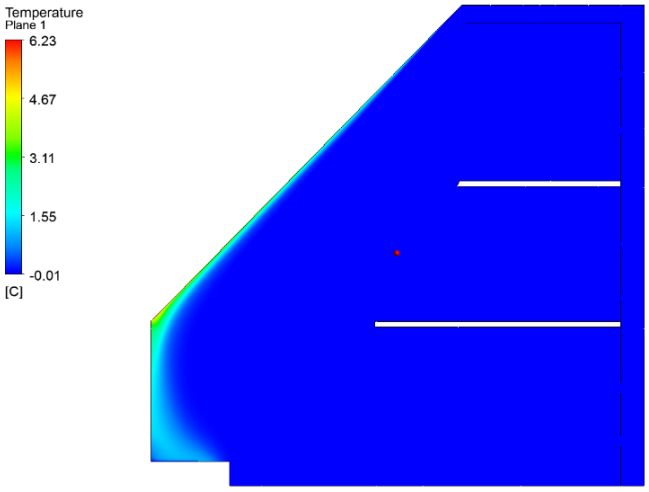

Figure 5.8 - temperature field after 120s, T_0 = 15ºC, v_0 = 2 m/s, T(inlet) = 0ºC, Q(glass) = 8.29 W/m²K, T(bottom) = 0ºC, with double sized entrances on the bottom of the perforated plate

As it can be seen in figure 3.14, the velocity was increased on the pretended zone, although there is still a small area where the velocity remains low. However, this also caused a reduction of the mass flow on the rest of the showcase (because the inlet

velocity/mass flow was maintained), which caused a slight increase of the temperatures overall (Figure 5.8). This is not critical in this particular case, but this model is not yet completed because the products and some other parameters that would affect negatively the performance were not considered yet.

Then, it can be concluded that this variation is not the best in a general case, but it can be a better solution if the products stored need ventilation.

5.2. Geometry with products inclusion and lamps influence

In this final stage, the products in the geometry will be introduced. These products have different dimensions and the bigger products are at the bottom because there is more space to place them (figure 5.9).

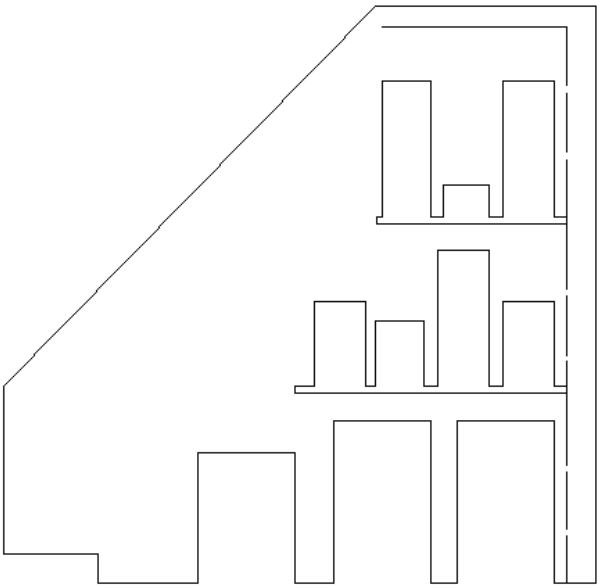

Figure 5.9 - geometry with products

On the bottom, the dimensions are 200 x 150 and 250 x 150 mm, respectively. On the shelves, the products are 70 to 80 mm wide, and 100 to 210 mm height, except the smaller one on the top shelf that is 50 mm height. The products have similar dimensions that some refrigerated food and drinks (packed products, water bottles,

soda cans, etc) and the gaps between have 20 mm or less. The point is to evaluate different situations where the space between the products are refrigerated or not.

The heat flux in the products will not be studied so there is no mesh in them, they act only as obstacles to the flow.

5.2.1. Mesh definition

The mesh definition is different from the previous ones because the introduction of products makes it impossible to produce the same mesh. The first change was the type of mesh: before it was a quadrilateral mesh and on this one is hybrid (with quadrilateral and triangular elements). In this geometry, the same technique shown in Figure 5.2 could not be used, so there are triangular elements near the glass (Figure 5.10). On the other hand, the elements on the rest of the geometry are quadrilateral and the principals followed on the mesh construction are the same, such as the element size being smaller near the wall because of the boundary layer.

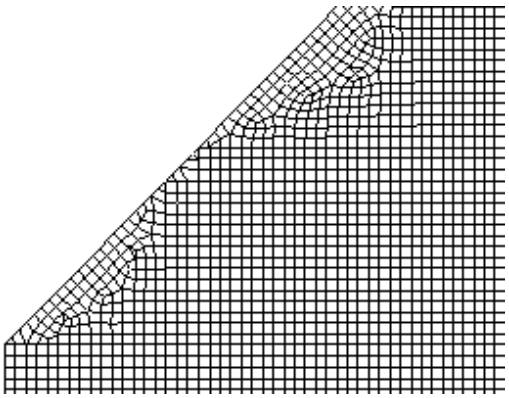

Figure 5.10 - mesh definition near the glass

In order to have the same precision, the element size is roughly the same, and not the total elements. This mesh has 70% fewer elements because there is no mesh on the products, which represents 30% of the total area.

5.2.2. Results

Figures 5.11 and 5.12 represents the simulation without and with the lamps' influence, respectively. The lamp is collocated near the air entrance on the top. Figure

5.13 represents the velocity field of both situations (the velocity results are the same, as expected).

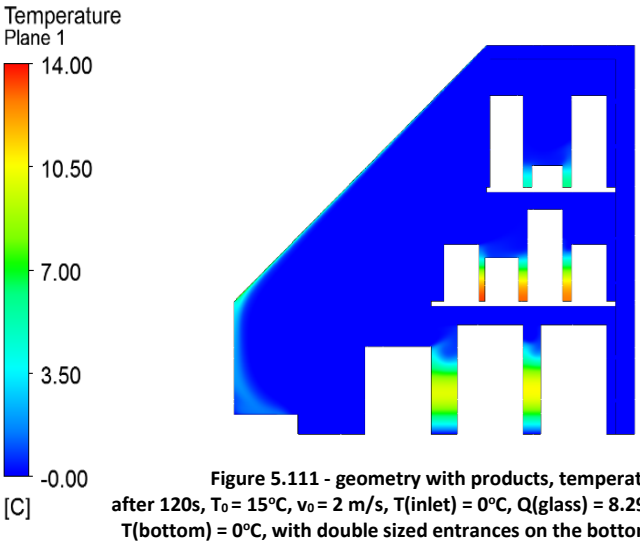

Figure 5.111 - geometry with products, temperature field after 120s, T_0 = 15ºC, v_0 = 2 m/s, T(inlet) = 0ºC, Q(glass) = 8.29 W/m²K, T(bottom) = 0ºC, with double sized entrances on the bottom of the perforated plate

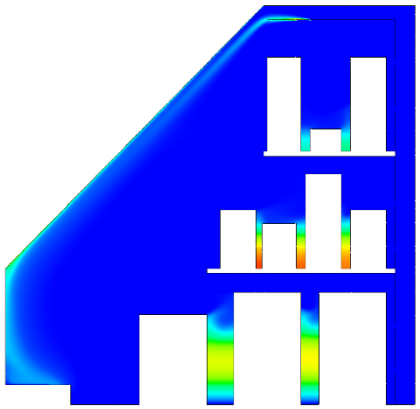

Figure 5.12 - lamps influence, geometry with products, temperature field after 120s, T_0 = 15ºC, v_0= 2 m/s, T(inlet) = 0ºC, Q(glass)= 8.29 W/m²K, T(bottom) = 0ºC, with double sized entrances on the bottom of the perforated plate

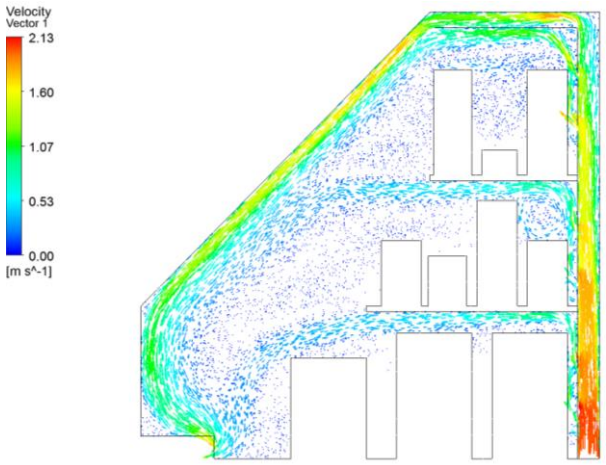

Figure 5.12 - geometry with products, velocity field after 120s, T_0 = 15ºC, v_0 = 2m/s, T(inlet) = 0ºC, Q(glass) = 8.29 W/m²K, T(bottom) = 0ºC, with double sized entrances on the bottom of the perforated plate

As it can be seen in Figures 5.11 and 5.12 the influence of the lamp is local, as it happened on the heat flux through the glass. The only propagation of the heat generation by the lamp is to the air curtain. As can also be seen on these figures, between the products there is almost no air flow, except on the top shelf between the first and third product. That means that in this zone the refrigeration will be reduced.

So, it can be concluded that 20 mm between the products is not enough to ventilate this space, a larger space was needed as there is on the top shelf, which is confirmed by figure 5.13 (the velocity is nearly 0 in the 20 mm gap).

However, there are a lot of limitations in the 2D simulations. Firstly, the gap between the products all the way across cannot be represented. That means that the air could be flowing the products, contrary to what is represented in oud 2D results. Secondly the inlet and outlets, so as the gaps in the back of the showcase, are represented as lines in 2D, which would be transposed to a rip all the way across. In the real geometry, the inlets, outlets and back perforation are often circular holes or oblongs, which can be only designed in a 3D geometry.

These limitations in the 2D geometry can leave us to some conclusions that are not true.

6. CONCLUSION AND FUTURE WORK

In this chapter some conclusion will be presented and the future work that would best complete this one.

6.1 Conclusions

This works contains some simulations with different conditions, where the first one is the simplest because it contains only the geometry itself, and the next simulations increase one more condition that were taken into account. The point of analysing the results this way is to visualize which condition has more impact on the temperature and/or velocity field and it becomes easier to see the errors on definition. If only the last case was made, it was not possible to verify the influence of each parameter.

The first case helped us to define the mesh definition for the following ones. At the beginning were used more than 1 mesh because it was not certain that the complexity of the next simulations would have different results, but it was concluded later that was not necessary.

The heat flux through the wall and the influence of the lamps' studies are similar in the way that it only affects locally for the values used.

On the other hand, defining the temperature as 0°C on the bottom wall (near the evaporator) affected a large area compared with the heat flux definition.

The last step on the empty showcase was to double the size on the bottom of the back perforated plate in order to increase the velocity on this area. It was concluded that by increasing the mass flow on the bottom, it will be reduced on the other entrances, causing to reduce the velocity of the airflow near the glass (air curtain). This might be interesting if depending on the application: if the products are packed, the first option is better because the temperature is lower overall, if there are products that need to be ventilated to maintain is properties, such as fruits and vegetables, it is better to use the second option.

Lastly, the geometry of the product is very limited because the products are represented by boxes, which have the same width as the showcase, that is not the real case, where the products are placed side-by-side, having enough space to the air circulate all the way across. This causes that the velocity is zero between the products, which is not true neither in width nor in length. For those reasons, where the products are included is suitable to develop a 3D simulation in order to get reliable results.

6.2 Future work

The future work to complement this one would be a 3D simulation that can represent better the reality and it would include more geometry changes, such as air entrances and exits, product dimensions and glass configuration, in order to optimize the configuration of the final equipment. The velocity inlet could also be analysed in order to minimize to reduce costs, always guaranteeing the temperature field remain acceptable. Another very important parameter that should be analysed is considering the products as a thermal load and not just an obstruction to the flow. As a final task, it could be done a prototype to validate all the results.

7. REFERENCES

[1] N. Chaomuang, D. Flick, and O. Laguerre, "Experimental and numerical investigation of the performance of retail refrigerated display cabinets," *Trends Food Sci. Technol.*, vol. 70, no. May 2017, pp. 95–104, 2017.

[2] P. Lobarinhas, "Ciclos Frigoríficos," in *Ciclos frigoríficos*, 2018.

[3] Leitão, B.M.R., "Equipamentos de congelação industrial de produtos alimentares perecíveis: análise comparada de apoio à decisão," Instituto Superior de Engenharia de Lisboa, 2015.

[4] PRODCOM, "NACE 13.10 : Mining of iron ores PRODCOM LIST 2006." p. 322, 2006.

[5] S. C. Ribeiro, "Estudo numérico de escoamentos em equipamento de refrigeração vertical aberto," Universidade do Minho, 2016.

[6] N. Chaomuang, D. Flick, A. Denis, and O. Laguerre, "Experimental analysis of heat transfer and airflow in a closed refrigerated display cabinet," *J. Food Eng.*, vol. 244, no. April 2018, pp. 101–114, 2019.

[7] L. Wang, L. Zhang, and G. Lian, "A CFD simulation of 3D air flow and temperature variation in refrigeration cabinet," *Procedia Eng.*, vol. 102, pp. 1599–1611, 2015.

[8] J.M. Belman-Flores, "Analysis of the flow and temperature distribution inside the compartment of a small refrigerator," *Appl. Therm. Eng.*, vol. 106, pp. 743–752, 2016.

[9] H. K. Versteeg and W. Malalasekera, *versteeg_computational_fluid_dynamics (2).pdf*. 1996.

[10] ANSYS, *"ANSYS FLUENT Theory Guide."* 2013.

[11] P. D. Gaspar, A. Miranda, and R. A. Pitarma, "Estudo numérico do escoamento de ar e do desempenho térrmico de equipamentos e expositores refrigerados," *Métodos Numéricos Ing. V*, p. 19, 2002.

[12] D. Parpas, C. Amaris, J. Sun, K. M. Tsamos, and S. A. Tassou, "Numerical study of air temperature distribution and refrigeration systems coupling for chilled food processing facilities," *Energy Procedia*, vol. 123, pp. 156–163, 2017.

[13] V. Guedes and D. Brás, "Simulação do escoamento numa vitrine de frio," 2018.

[14] J. Sun, K. M. Tsamos, and S. A. Tassou, "CFD comparisons of open-type refrigerated display cabinets with/without air guiding strips," *Energy Procedia*, vol. 123, pp. 54–61, 2017.

[15] F. Casa, "No Title," *O vidro e o isolamento térmico*, 2019. [Online]. Available: https://forumdacasa.com/discussions/?PostBackAction=Download&AttachmentID=1069: . [Accessed: 21-Oct-2019].